JULY 2017 M.Sc. in Mechanical Engineering MEHMET MUMBUÇOĞLU

UNIVERSITY OF GAZİANTEP
GRADUATE SCHOOL OF
NATURAL & APPLIED SCIENCES

ANALYSIS OF WARM FORMING OF LOCALLY HEATED SHEET METALS BY USING FINITE ELEMENT METHOD

M. Sc. THESIS
IN
MECHANICAL ENGINEERING

BY
MEHMET MUMBUÇOĞLU
JULY 2017

Analysis of Warm Forming of Locally Heated Sheet Metals by Using Finite Element Method

M.Sc. Thesis

in

Mechanical Engineering

University of Gaziantep

Supervisor

Prof. Dr. Ömer EYERCİOĞLU

by

Mehmet MUMBUÇOĞLU

July 2017

REPUBLIC OF TURKEY
UNIVERSITY OF GAZİANTEP
GRADUATE SCHOOL OF NATURAL & APPLIED SCIENCES
MECHANICAL ENGINEERING

Name of the thesis: Analysis of Warm Forming of Locally Heated Sheet Metals by Using Finite Element Method
Name of the student: Mehmet MUMBUÇOĞLU
Exam date: 11.07.2017

Approval of the Graduate School of Natural and Applied Sciences

Prof. Dr. A. Necmeddin YAZICI

Director

I certify that this thesis satisfies all the requirements as a thesis for the degree of Master of Science.

Prof. Dr. Sait SÖYLEMEZ

Head of Department

This is to certify that we have read this thesis and that in our consensus opinion it is fully adequate, in scope and quality, as a thesis for the degree of Master of Science.

Prof. Dr. Ömer EYERCİOĞLU

Supervisor

Examining Committee Members	Signature
Prof. Dr. İ. Hüseyin FİLİZ	.....
Prof. Dr. Abdulkadir EKŞİ	.....
Prof. Dr. Ömer EYERCİOĞLU	.....
Assoc. Prof. Dr. Necip Fazıl YILMAZ	.....
Assoc. Prof. Dr. A. Tolga BOZDANA	.....

I hereby declare that all information in this document has been obtained and presented in accordance with academic rules and ethical conduct. I also declare that, as required by these rules and conduct, I have fully cited and referenced all material and results that are not original to this work.

Mehmet MUMBUÇOĞLU

ABSTRACT

ANALYSIS OF WARM FORMING OF LOCALLY HEATED SHEET METALS BY USING FINITE ELEMENT ANALYSIS

MUMBUÇOĞLU, MEHMET
M.Sc. in Mechanical Engineering Department
Supervisor: Prof. Dr. Ömer EYERCİOĞLU
July 2017
66 pages

Automotive industry uses stainless steels for place where needed corrosion resistance and aluminum or magnesium alloys to reduce weight of chassis. High mechanical properties of these materials are reasons for preference however low formability of these materials in the ambient temperature creates manufacturing problems. In this study, enhancement of bending ability of a stainless steel and a magnesium alloy by local heating was investigated. The specimens were bent in V-bending die by using a servo-press at room temperature. Load and deformation rate were determined during forming process. Final shapes were measured by Coordinate Measuring Machine (CMM) and springback ratios were determined. Same procedures were conducted with locally heating (heating the region of deformation) and the results were compared with cold forming. It was observed that locally heating the bending area was adequate to give form the workpiece and this result was verified with FEM. The changing of the thickness on the bending area was also determined for cold and locally heated specimens.

Keywords: Locally Heating, Formability, Stainless Steel, Magnesium Alloy, FEM.

ÖZET

SONLU ELEMAN METHODU KULLANILARAK LOKAL OLARAK ISITILMIŞ SAC LEVHALARIN ILIK ŞEKİLLENDİRİLMESİNİN ANALİZİ

MUMBUÇOĞLU, MEHMET
Yüksek Lisans, Makine Mühendisliği Bölümü
Tez Yöneticisi: Prof. Dr. Ömer EYERCİOĞLU
Temmuz 2017
66 sayfa

Otomotiv endüstrisi paslanmaya karşı mukavemete ihtiyaç duyduğu yerlerde paslanmaz çelik, şasinin ağırlığı azaltmak için ise alüminyum veya magnezyum alaşımları kullanmaktadır. Yüksek mekanik özellikleri bu malzemeler için tercih sebebi iken oda sıcaklığında şekillendirilebilme kabiliyetinin düşük olmasından dolayı imalatta problemler oluşturmaktadır. Bu çalışmada, paslanmaz çeliğin ve magnezyum alaşımının bölgesel ısıtma ile bükülme kabiliyetindeki artış incelenmiştir. Parça oda sıcaklığında V bükme kalıbında bir servo-pres kullanılarak bükülmüştür. Yük ve deformasyon oranı büküm işlemi boyunca saptanmıştır. Son şekiller koordinat ölçme makinesi ile ölçülmüş ve geri yaylanma oranı belirlenmiştir. Aynı işlemler bölgesini ısıtma (büküm bölgesisin ısıtılması) ile de gerçekleştirilmiş ve sonuçlar soğuk şekillendirme ile karşılaştırılmıştır. Büküm alanını bölgesel olarak ısıtmanın iş parçasına şekil vermek için yeterli olduğu gözlemlenmiş ve bu sonuç sonlu eleman analizleri ile doğrulanmıştır. Bölgesel olarak ısıtılarak ve soğuk halde bükülmüş parçalardaki kalınlık değişimleri de belirlenmiştir.

Anahtar Kelimeler: Local ısıtma, şekillendirilebilirlik, paslanmaz çelik, magnezyum alaşımı, sonlu eleman methodu

To My Parents

ACKNOWLEDGEMENTS

Firstly, I am very grateful to my supervisor Prof. Dr. Ömer EYERCİOĞLU for his continuous support during my M. Sc. study and research, for his patience, motivation, enthusiasm and immense knowledge. It has been an honour to be his student.

I also thank to my friend Research Assistant Mahmut TANDOĞAN and my Manager Kerem ELİBAL for their supports and motivations.

Deepest gratitude is to my parents, for their endless support, interest and prays.

TABLE OF CONTENTS

Page

LIST OF TABLES

Page

LIST OF FIGURES

Page

LIST OF SYMBOLS/ABREVIATIONS

$\boldsymbol{\alpha}$	Bending Angle
$\boldsymbol{\sigma}$	True Stress
$\boldsymbol{\sigma_E}$	The Effective Stress
$\boldsymbol{\sigma_{max}}$	The Maximum Principal Stress
$\boldsymbol{\sigma_y}$	Yield Stress
℃	Celsius
$\boldsymbol{D_r}$	Deep Drawing Ratio
$\boldsymbol{\varepsilon_f}$	The Limit Fracture Strain
E	Modulus of Elasticity
$\boldsymbol{\varepsilon}$	Strain
$\boldsymbol{\varepsilon_{pl}}$	The Plastic Strain
F	Force
K	Kelvin
$\boldsymbol{K, C}$	Material Constants
L	Length of Bending Line
$\boldsymbol{L_b}$	Bending Allowance
$\boldsymbol{n}$	Strain Hardening Coefficient
$\boldsymbol{s^{-1}}$	Strain Rate
R	Radius of Curvature
$\mathbf{r_0}$	Initial Blank Radius
$\mathbf{r_p}$	Punch Radius

$\mathbf{S_{ut}}$	Ultimate Tensile Stress
t	Thickness
DIN	German Institute for Standardization
FEM	Finite Element Method
BHP	Blank Holder Pressure
NIR	Near-Infrared Ray
SEM	Scanning Electron Microscope
OM	Optical Microscope
FLD	Forming Limit Diagram
ECAE	Equal Channel Angular Extrusion
LDR	Limit Drawing Ratio
HPT	High Pressure Torsion
GPa	Giga pascal
ISO	International Organization for Standardization
HCP	Hexagonal Closed Packed
CRSS	Critical Resolved Shear Stress
SAFSS	Structural Applications of Ferritic Stainless Steels

CHAPTER 1

INTRODUCTION

In automobiles, presently 15-22 kilograms of stainless steels are used [1]. There are some applications where the chassis is completely produced from stainless steels. Since corrosion resistance remains fundamental requirement for these applications, selection of grades and stabilizing elements are critical for such applications and depend primarily on operating conditions. Stainless steels are also being used in other applications such as fuel tank, mudguard, chassis for buses and trucks. With the development of new varieties of austenitic, ferritic and martensitic stainless steels, automotive industry is intensively exploring their potential [2].

Applications of magnesium in the automotive industry can significantly contribute to greater fuel economy. The usage of magnesium in automotive applications is also assessed for the impact on environmental conservation. Recent developments in coating and alloying of Mg improved the creep and corrosion resistance properties of magnesium alloys for elevated temperature and corrosive environments [3].

DIN 8580 classifies manufacturing processes in 6 main groups: changing of material property, coating, joining, casting, cutting and forming. Forming is defined as manufacturing through the plastic modification or three dimensional of a shape while conserving its mass and material cohesion by DIN 8580. Forming is classified by DIN 8582 according to main direction of applied stress on the material and DIN 8586 investigates forming by bending. DIN 8586 divided into two groups: bending with linear die movement and bending with rotary die movement.

Temperature of forming process has important role on formability. In sheet metal cold forming process larger force is required than warm ($0.35T_m < T < 0.55T_m$) and hot forming because of high flow stress value and low ductility. Hot forming is not a proper choice due to surface deterioration because of oxidation and scale formation. In hot forming, whole part is heated. But this is not economical process and time consuming. These problems can be overcome with local warm forming. Local warm forming does not require force as high as cold forming of sheet metal and it is possible to obtain closer dimensional tolerances since the entire sheet metal is not heated.

In this study, numerical modelling and experimental investigation of locally warm forming of sheet metal with linear bending die movement are carried out. For this purpose sheet metal bending specimens are modelled by using finite element method and warm forming analyses are done. The experimental studies are carried out to determine boundary conditions of finite element analyses.

This thesis consists of seven chapters; literature review, sheet metal forming, experimental studies, finite element modelling, result and discussion and conclusions. In literature review, Chapter 2, studies related with locally heating and behaviour of sheet metals at elevated temperatures are briefed. Basic theoretical formulation required for sheet metal forming is given in Chapter 3. Chapter 4 describes the experimental study of this thesis. Finite element modelling and simulations are given in Chapter 5. The results of experimental studies and finite element analyses are discussed in Chapter 6. In the last chapter, Chapter 7, conclusions derived from the study and recommendations for future work are given.

CHAPTER 2

LITERATURE REVIEW

Formability of sheet metals is generally investigated in terms of temperature and strain rate. Studies have shown that formability is directly related with process parameters. So researchers concentrated on relation between formability and these process parameters (temperature, strain rate, lubrication). While some studies focus on temperature or strain rate effect on formability individually, there are a lot of studies investigate temperature and strain rate effect at the same time.

Most of the studies related to temperature effect on formability is about completely heating of workpiece, but this study is focused on the effect of locally heating on formability. So this chapter is divided into two sections: review on behaviour of sheet metals under *local heating* and review on formability of sheet metals *at elevated temperature.* The section includes summary of previous studies that are investigate the effect of completely heating of specimens on formability.

2.1 Reviews on Behaviors of Sheet Metals under Local Heating

There are a lot of studies about formability of magnesium alloys (commonly AZ31B and AZ91B) at elevated temperatures based on the fact that magnesium alloys have poor formability at room temperature due to its microstructure and formability increases directly proportional to certain temperature.

Yoshihara et al. [4] (2004) studied on new deep drawing operation to form magnesium alloy which is not possible to achieve by conventional deep drawing method. In this technique, firstly blank is hold between the die and the blank holder which are including heater units. Punch moves down at a certain strain rate

(200 mm/min) by pressing workpiece. During this operation unformed part of workpiece was heated and formed part of workpiece was cooled by water injection as shown in Figure 2.1. So locally heating operation was conducted. Optimisation of deep drawing process, temperature distribution and formability were studied. Same operation was applied with locally heating and cooling system using finite element simulation (ANSYS/LS-DYNA). Magnesium alloy was deep drawn with changing cooling water and blank holder pressure (BHP) without changing the deep drawing ratio and drawn-cup height 90mm. Experimental results of this study were confirmed by FEM simulations.

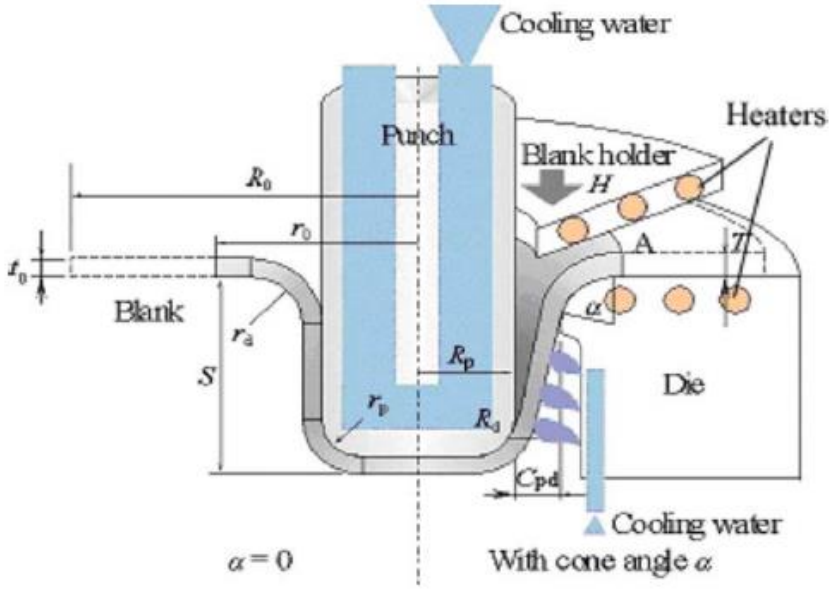

Figure 2.1 Schematic of Circular-Cup Deep-Drawing System with Local Heating and Cooling

Eun-Ho Lee et al. [5] (2014) exhibit advantages of locally heating on springback of non-quenchable advanced high-strength steels. In the mentioned study Near-Infrared Ray (NIR) method was used for local heating the specimens. Special devices were designed to obtain regular heating on the specimen. These devices lead heating energy on the specimen bending area as shown in Figure 2.2. Specimens were locally and completely heated up to different temperatures (20^0C, 200^0C, 400^0C, 600^0C and 700^0C). Hardness, springback and microstructural changing of specimens were compared for locally and completely heating conditions.

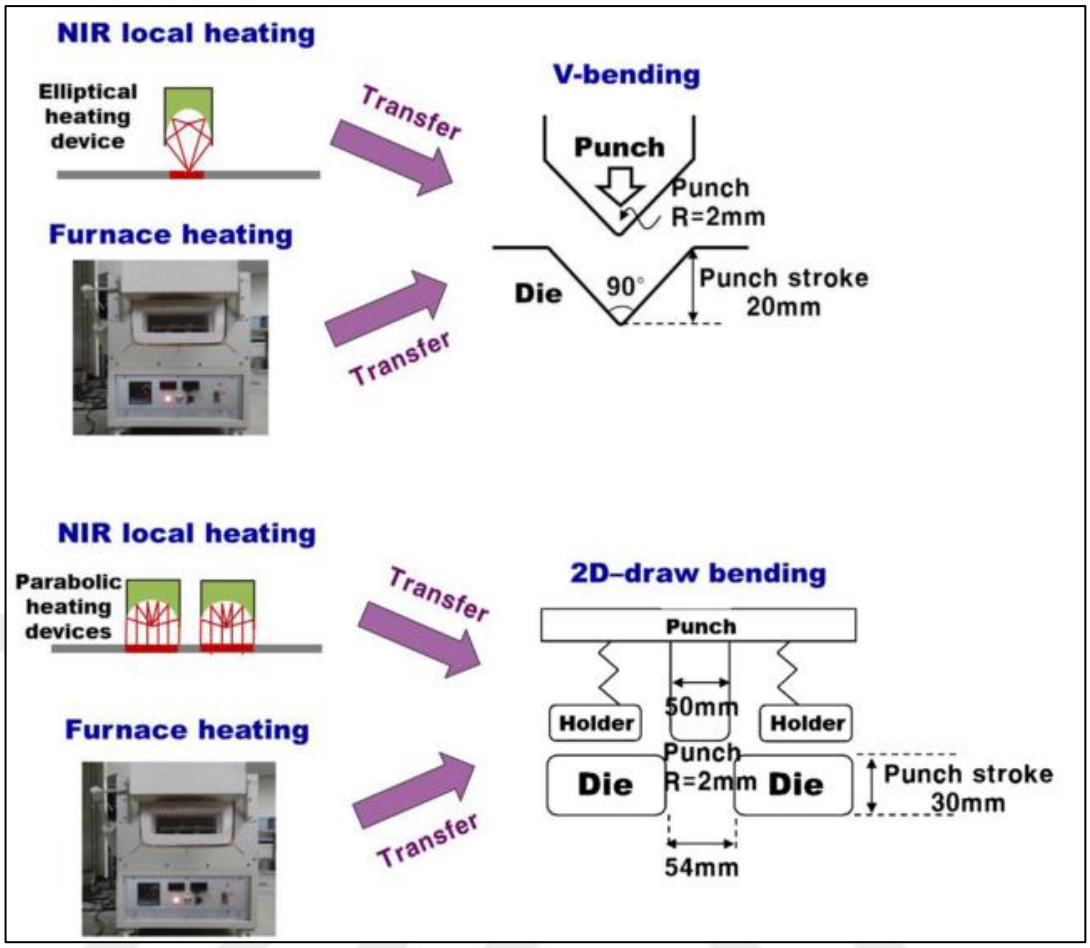

Figure 2.2 Locally Heating Devices

Hıno et al. [6] (2008) studied on a new incremental sheet metal forming method and aimed to shape difficult to form materials (A5083 and AZ31). In this method, workpiece was held between blank holders and die rotated counter-clockwise and then rotated clockwise as shown in Figure 2.3. Punch has built-in heating unit and moves perpendicular to workpiece surface. During formation operation temperature of workpiece was increased up to 875 K. This gradually turning and translating movement continues until final shape was obtained. By forming, 15^{o} and 25^{o} cone angles were achieved for A5083 and AZ31 materials with this method.

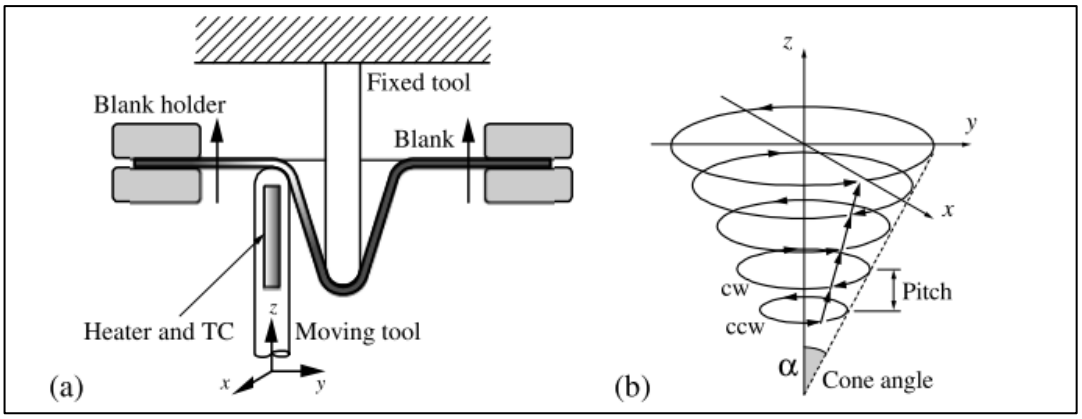

Figure 2.3 Schematic Illustrations of (a) Incremental Sheet Forming with Local Heating Using Moving Tool and Fixed Tool, and (b) Tool Path for Cone-Shape Forming Experiment

Kim et al. [7] (2017) compared formability of locally heated AZ31 circular sheet by using Erichsen test with a different temperature and strain rate values and took into account fracture failure criteria (N.Cockroft, Brozzo and Ayada). Experimental and theoretical results were overlapped with Cockroft-Latham criteria.

2.2 Reviews on Increasing Formability of Sheet Metals at High Temperatures

Tokita et al. [8] (2017) studied on stretch formability of high strength steels at warm temperature. Galvanized and annealed steels have been formed by spherical stretch forming test apparatus at different temperatures between room temperature and 600°C. Initial experiments showed that in warm forming maximum formable dome height without cracks is lower than cold forming even though, material strength reduces at elevated temperature. Reason of this poor stretch formability is explained with surface temperature and strain in spherical stretch forming test apparatus.

Ebrahimi et al. [9] (2012) studied on microstructure of magnesium alloy (AZ91) at high temperatures. Hot compression test was conducted at a temperature changing from $350°C$ and $425°C$ and at strain rate from $0.1s^{-1}$ to $0.5s^{-1}$. It is observed that entire conducted temperatures, by increasing strain, the number of recrystallized grains first increases and they reaches a maximum value and then decreases. The change in microstructure of magnesium alloy was observed using Scanning Electron Microscope (SEM) and Optical Microscope (OM).

Bong et al. [10] (2013) researched formability of austenitic and ferritic stainless steel at warm forming temperature. Two different groups was drawn with different technique. While first group punch, die and holder heated up to observe effect of fully heating on specimen, in second group holder and die were heated up but punch was cooled to delay localized thinning.

Mabuchi et al. [11] (1997) worked on low temperature superplasticity of AZ91 magnesium alloy processed by Equal Channel Angular Extrusion (ECAE). In this study, AZ91 having 1 μm and 37 μm grain sizes were processed to investigate effect of grain size on superplasticity. Tensile tests were conducted at different temperatures. It was found that 661% elongation was observed at 473 K with $6.2x10^{-5}s^{-1}$.

Zhang et al. [12] (2006) analysed the formability of AZ31 magnesium alloy at warm working temperature. Firstly, the sample was hot rolled to obtain fine-grained microstructure and then uniaxial tensile tests were conducted at various temperatures and strain rates to investigate the mechanical properties. Limit dome height (LDH) and Limit drawing ratio (LDR) tests were conducted at temperatures changes between $50°C$ and $240°C$. Maximum LDR reaches 2.65 at the punch speed of 30 mm/min and $200°C$, however the maximum LHD is 10.8 mm. This result shows AZ31 has good deep drawability but poor stretchability. At same time punch speeds and punch temperatures were found to have important effects on the formability of AZ31 magnesium alloy sheets.

Ji et al. [13] (2008) studied on formability of AZ31 sheet in the incremental forming at warm temperature. To evaluate the increasing formability of specimen forming limit, plane-strain, as well as axisymmetric stretching test were conducted at $20°C$, $100°C$, $150°C$, $200°C$, and $250°C$. Cones with different inclination angles were designed based on the forming limits at these temperatures, and formed incrementally.

Al-Zubaydi et al. [14] (2015) investigated superplastic behaviour of AZ91.For this reason one disk which has 0.6 mm thickness and 10 mm diameter was placed into High Pressure Torsion (HPT) test apparatus and test was conducted at room temperature, at speed of 1rpm using applied pressure of 3 GPa for differing number of turns (1, 3, 5, 10 turns). Miniature tensile test sample (1 mm x 0.9 mm x 0.6 mm) was cut from the disk to operate tensile test. Tensile tests were conducted at different strain rates and temperatures; the highest value of elongation was observed 1308% for 573 K and 10^{-4} s^{-1} as shown in Figure 2.4

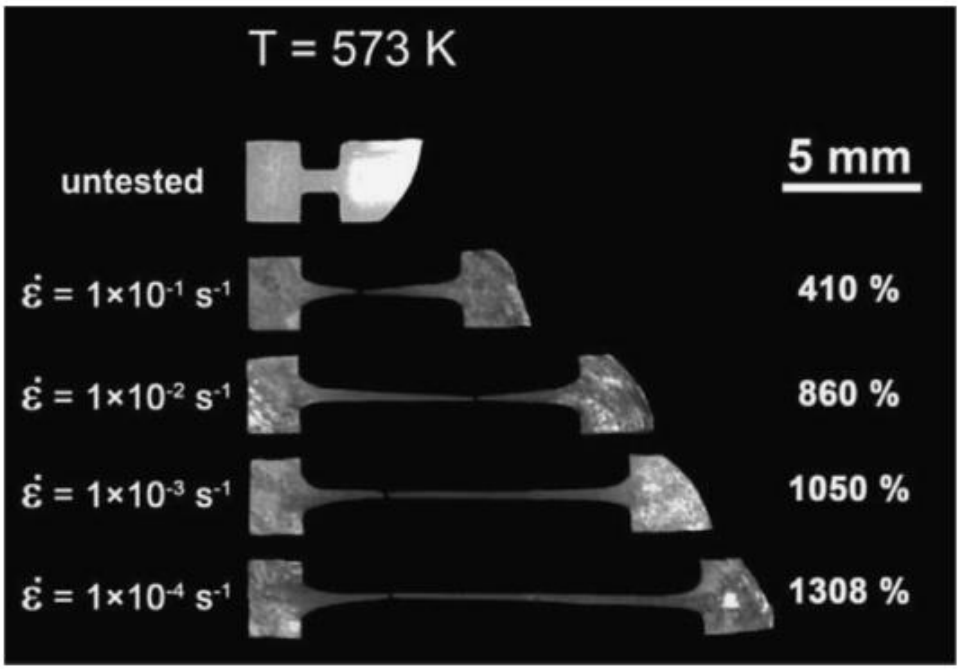

Figure 2.4 Appearances of Samples Processed by HPT for 10 Turns After Tension to Fracture at a Testing Temperature of 573 K at Different Strain Rates. The Upper Sample Represents The Untested Case

Kim et al.[15] (2010) investigated failure of AZ31 under consideration of different process parameters (temperature and strain rate values) which has been incorporated based on developed linear correlation and three different ductile criterias Cockroft-Latham, Normalized Cockroft-Latham and Freudenthal.

CHAPTER 3

SHEET METAL FORMING

Metal forming process can be classified into two main groups as bulk metal forming and sheet metal forming. The difference comes from the ratio of volume to surface area of the workpiece material. The ratio is smaller in sheet metal forming and generally the thickness of the workpiece material is less than 6mm. The behaviour of sheet metal and mathematical expression of this behaviour should be known to analyse the sheet metal forming process. A brief description of the forming behaviour of the sheet metal is given in this section.

3.1 Flow Stress and Effects of Strain Rate and Temperature

In sheet metal forming, flow stress of the material is used in determination of the forming load. There are a lot of theories to calculate flow stress. Hollomon equation is the most popular and the simplest. The Hollomon equation defines flow stress as:

$$\sigma = K_1 . \varepsilon^n \qquad (\mathbf{3.1})$$

where σ is the flow stress, K is a material constant, ε is the true strain and n is the strain hardening coefficient. In the equation "n" value is obtained from slope of log σ- log ε curve and it is commonly used for stretch formability of material. Strain hardening is strengthening of the metal by plastic deformation and

this is occurred due to dislocation movement and dislocation generation. It is not accurate for some materials (iron, 1.4003, etc.) because of nonlinearity of log σ- log ε curve. To overcome this problem the Holloman equation was revised as given in equations 3.2 and 3.3.

$$\sigma = K_1.\varepsilon^{n_1} \quad \varepsilon_{lu} \leq \varepsilon \leq \varepsilon_1 \tag{3.2}$$

$$\sigma = K_2.\varepsilon^{n_2} \quad \varepsilon_1 \leq \varepsilon \leq \varepsilon_n \tag{3.3}$$

where ε_{lu} is Lüder strain and K_1, K_2, n_1, n_2 are constants. These two equations correspond to two straight lines on log σ- log ε and they intercept at point ε_1 as shown in Figure 3.1.

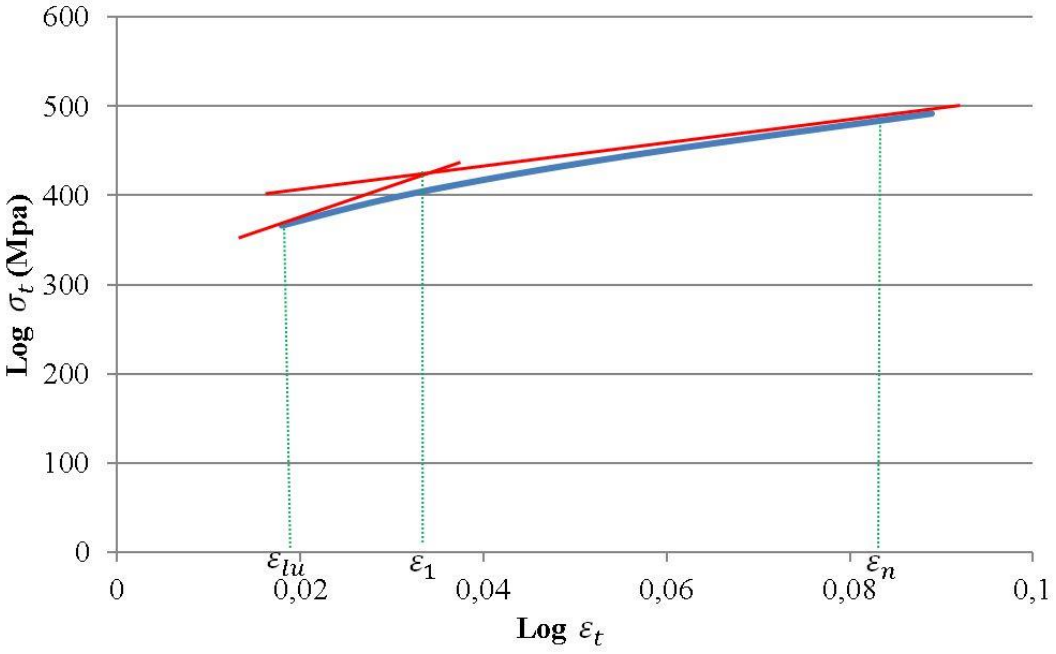

Figure 3.1 Log True Stress- Log True Strain Curve

The Holloman equation is valid for homogenous deformation region but in plastic deformation of a tensile specimen there are 3 regions; strain hardening, necking and fracture. Necking is a mode of tensile deformation where relatively large amounts of strain in a small region of the material. Fracture is defined as division of the pieces

under the action of stress. Fractured region of material after tensile test gives an idea about whether material is ductile or brittle.

Strain rate and temperature are effective parameters in plastic deformation. Below recrystallization temperature, strain rate is less effective on flow stress for metals. Changing in flow stress according to strain rate and temperature is given 3-D graph for 42CrMo high strength steel in Figure 3.2.

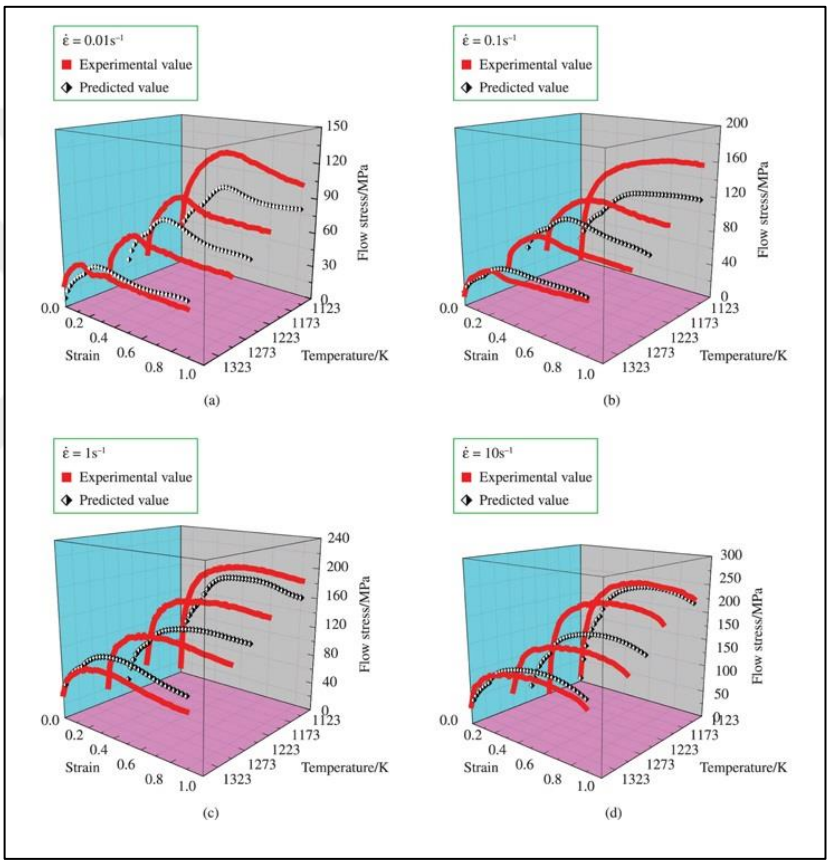

Figure 3.2 Flow Stress Behaviour of 42CrMo High Strength Steel in Despite of Temperature and Strain at Constant Strain Rate [16]

3.2 Forming Limit Curve

In sheet metal forming process, deformation is measured as relation between principal strains (minor and major strains). Formability can be interpreted by using minor and major strains. Tensile test is not adequate due to instability for complex strain states; in such cases Forming Limit Diagram is used.

Forming Limit Curve (FLC) is obtained by following these steps; firstly, specimen is marked with circles on the surface where test will be conducted. The specimen is loaded by a hemispherical punch moves until cracking start and surface where has been a marked swell. Circles on the surface turn into ellipses as shown in Figure 3.3. Relative strains in two primary directions are measured by optical strain measurement system and measured values are marked on forming limit axis. All procedure should be carried out according to ISO 12004.

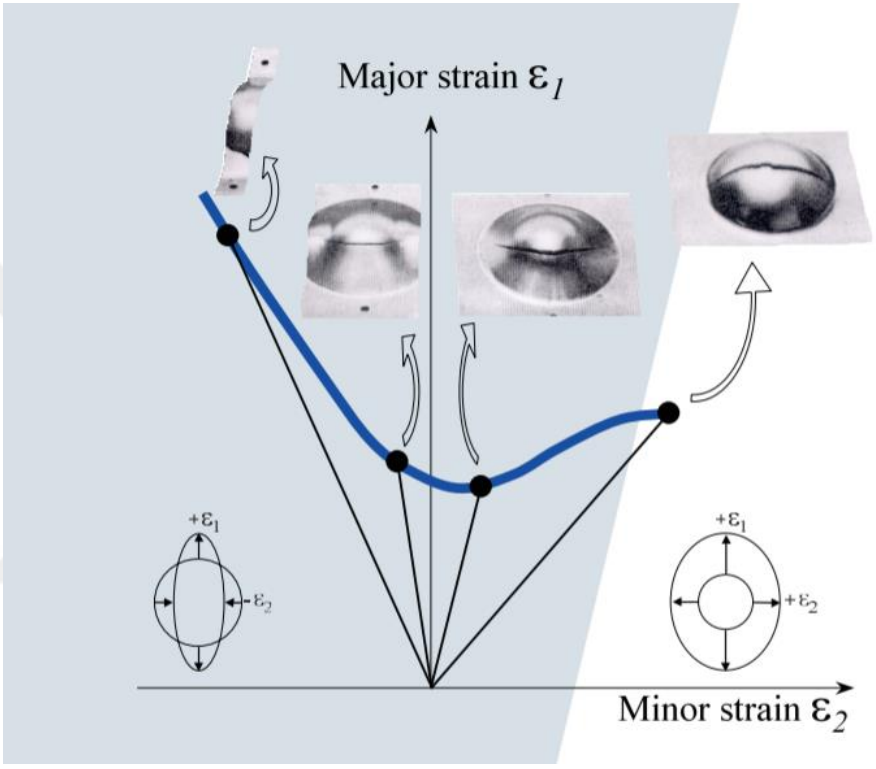

Figure 3.3 An Example of a FLD for Uniform Deformation [17]

As mentioned above formability is related with strain state. Strain state is determined according to principal strains (ε_1, ε_2 and ε_3). Summation of these three principal strains is assumed as zero, so only ε_1 and ε_2 is adequate to describe strain state. Relation between ε_1 and ε_2 is expressed as;

$$\varepsilon_2 = \beta . \varepsilon_1 \qquad (\mathbf{3.4})$$

β is a constant value can be positive or negative and it describes state of strains.

$\beta = -1$; $\varepsilon_2 + \varepsilon_1 = 0$ and attendantly $\varepsilon_3 = 0$, there is no change in thickness and this case presents that flange of deep-drawn products.

$\beta = -0.5$; This case states material is non-isotropic,

$\beta = 0$; There is no second principal strain ($\varepsilon_2 = 0$),

$\beta = 1$, $\varepsilon_1 = \varepsilon_2$ and this case is called as equi-biaxial because strain is constant on the surface.

3.3 Bending

Bending is one kind of forming operation which applied bending stress turns a flat straight sheet into curved object. While using a press brake and standard die sets, there are still a variety of techniques that can be used to bend the sheet. The most common method is known as V-bending, in which the punch and die are "V" shaped. The punch pushes the sheet into the "V" shaped groove in the V-die, causing it to bend. If the punch does not force the sheet to the bottom of the die cavity, leaving space or air underneath, it is called "air bending". As a result, the V-groove must have a sharper angle than the angle being formed in the sheet. If the punch forces the sheet to the bottom of the die cavity, it is called "bottoming" as shown in Figure 3.4. This technique allows for more control over the angle because there is less springback. However, a higher tonnage press is required. In both techniques, the width of the "V" shaped groove, or die opening, is typically 6 to 18 times the sheet thickness. This value is referred to as the die ratio and is equal to the die opening divided by the sheet thickness. If die and punch have V- shape, bending operation is called as V-bending. [18]

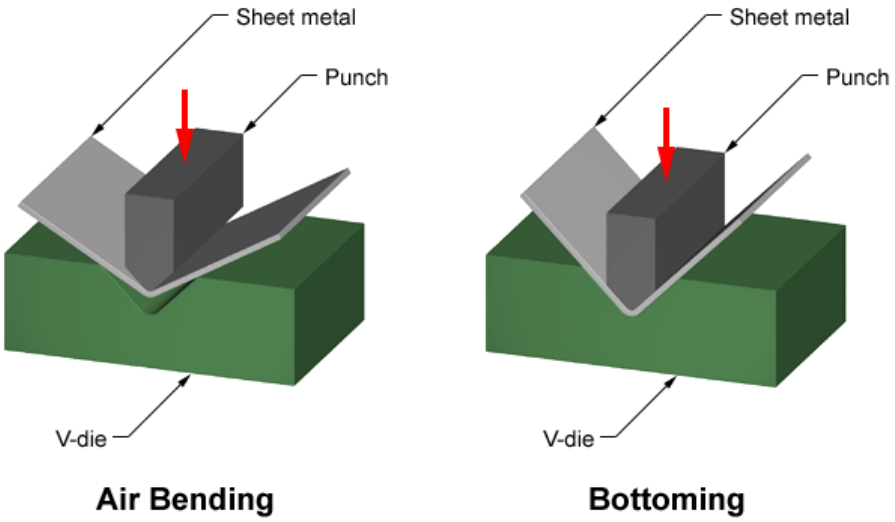

Figure 3.4 Illustration of Air Bending and Bottoming [19]

The larger V opening the larger the radius, so inside radius of workpiece is set by V opening. This explains why air bending tonnage is less then bottoming. Operator can control inside radius of workpiece by changing stroke of punch. This can be problem for design options because inside radius of finished part is not equal to punch tip radius. Inside radius of workpiece is determined by V opening of the die not by the punch tip radius. Commonly acute angle tooling is used to form sheet metal in air bending. Springback effect is observed clearly in air bending.

3.3.1 Bending Allowance and Minimum Bend Radius

Bending has multiple effects on the material. During bending the outer surface of the workpiece is in tension and the inner surface is in compression. While in elastic bending process neutral axis places centre of thickness of material, in plastic deformation neutral axis shifts inside of the bend.

For the sake of simplicity, thickness reduction is neglected. Consider a sheet metal of thickness "t" and radius of curvature is "R" and "a" is an angle of bend. Strain along width direction can be neglected if w>>t. Length of bending arc between tangent points on the outer side of any bend workpiece is called as bending allowance (L_b). It is an important design parameter and calculated as [20]:

$$L_b = a(R + Kt) \qquad (\mathbf{3.5})$$

where K is a constant,

$$K = 0.33 \text{ for R} < 2\text{t}$$
$$K = 0.5 \text{ for R} > 2\text{t}$$

For ideal bending radius inner strain fibre is equal to outer strain fibre. It can be written as [20];

$$\boldsymbol{\varepsilon} = \frac{1}{\left(\frac{2R}{t}\right) + 1} \qquad (\mathbf{3.6})$$

But in practice, while outer fibres stretches and the inner fibres getting shrunk. Difference between outer and inner fibres increases with reducing in radius of bending. Cracking starts when outer tensile strain fibres reach the critical value.

Minimum bend radius is zero means that sheet metal can be bent on itself (hemming). In order to obtain an expression for minimum bend radius, the true strain of a material during uniaxial tensile test at fracture can be equated to the strain in bending [20].

$$In\left(\frac{A_0}{A_f}\right) = In(1 + e) = In\left(1 + \frac{1}{\left(\frac{2R}{t}\right) + 1}\right) \qquad (\mathbf{3.7})$$

$$\left(\frac{R}{t}\right)_{min} = \frac{1}{2r} - 1 \qquad (\mathbf{3.8})$$

where r is reduction in area of the sheet during bending operation. For hemming process reduction in area is 50%.

Ductility of material is important phenomena for bending operation. Ductility and minimum bend radius are inversely proportional. If ductility is high R_{min} is low, if ductility is low R_{min} is high. Biaxial stress in the fiber at outer surface in bend region reduces ductility.

Bendability can be improved by applying the material to hydrostatic stress. Induced compressive stress on the outside of workpiece may also increase bendability. Rough edge and anisotropy have detrimental effect on the bendability of the outer surface.

3.3.2 Springback

Elastic recovery of the sheet after the bend load is removed is called springback. Illustration of springback is shown in Figure 3.5. This phenomenon may be observed in plastic deformation of ductile materials. Springback should be considered when designing a die because springback reduces bend angle. It is more important for materials that have low elastic modulus and/or high yield strength. This condition frequently observed when material has high value of width to thickness ratio. While bend allowance doesn't change after releasing the load, however bend radius changes.

$$L_b = a_i(R_i + Kt) = a_f\big(R_f + Kt\big) \qquad (\mathbf{3}.9)$$

$$K = \frac{a_f}{a_i} = \frac{(\frac{2R_i}{t} + 1)}{(\frac{2R_f}{t} + 1)} \qquad (\mathbf{3.10})$$

where K is springback factor, R_i is initial radius of curvature before releasing the load, R_f is radius of curvature of bend after releasing the load. $K = 1$ means material is totally elastic recovery like spring. $K = 0$ means there is no springback. Springback is inversely proportional to $\frac{R}{t}$ ratio. If $\frac{R}{t}$ ratio increases springback decreases. Bend radius and springback relation is formulated as in equation 3.11 [20].

$$\frac{R_i}{R_f} = 4(\frac{R_i.Y}{E.t})^3 - 3\left(\frac{R_i.Y}{E.t}\right) + 1 \qquad (\mathbf{3.11})$$

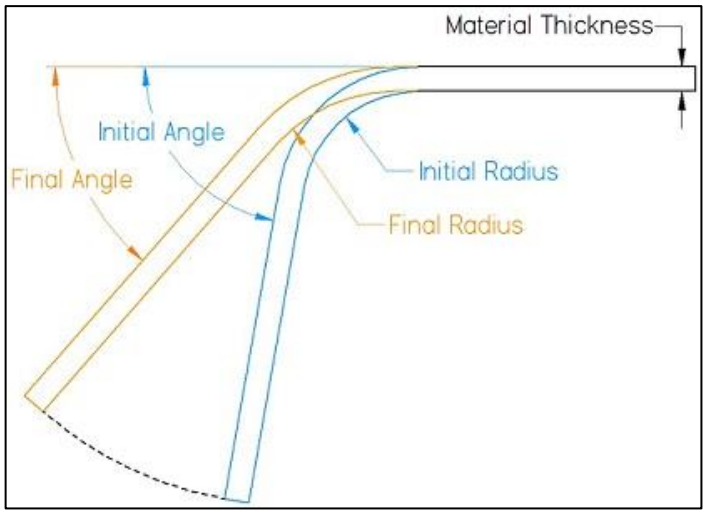

Figure 3.5 Illustration of Springback [21]

3.3.3 Bending Force

Force required for bending is given by [20];

$$F = \frac{YLt^2}{2(R + \frac{t}{2})} \tan\left(\frac{a}{2}\right) \qquad (\mathbf{3.12})$$

The maximum bending force formulation written in equation 3.13 is used in condition which the punch-tip radius and the sheet thickness are relatively small compared to die opening.

The maximum bend force is calculated with following equation [20];

$$F_{max} = \frac{kS_{ut}Lt^2}{W} \qquad (\mathbf{3.13})$$

S_{ut}= Ultimate tensile strength

W =V die opening width

k value is 1.3 for V-bending and 0.3 for wiping.

CHAPTER 4

EXPERIMENTAL STUDIES

4.1 Introduction

In this chapter, properties of the workpiece material, experimental procedure and equipment used in this study are explained.

4.2 Workpiece Materials

In this study AZ91B magnesium alloy and 1.4003 stainless steel have been used as workpiece materials. Both of these materials are purposely selected as they are difficult to form. AZ91B magnesium alloy is very sensitive to temperature and generally worked out at elevated temperatures. 1.4003 stainless steel is one of the mostly used materials in automobile components. Therefore, the feasibility of forming by local heating is studied.

4.2.1 AZ91B Magnesium Alloy

Magnesium is one of the most abundant metal elements in the earth. The most important characteristic of magnesium is its low density, 1.74 g/cm^3. Magnesium has a higher specific strength and stiffness than many other engineering materials, including aluminium, steel and polymer-based composites [22]. These properties make it attractive for many industrial applications. Aerospace, information and communication technology, medical and automotive industries have been using magnesium alloys with an increasing amount by years.

In automotive industry, usage of magnesium alloy is initiated in 1920's. Volkswagen group have saved around 14 kilograms by using AZ series magnesium casting alloy in Passat, Audi A4 and A6. General Motors (GM) and Ford have used magnesium alloys at different places in motor vehicles since the 1970s as illustrated in Figure 4.1. They and United States Council Automotive Research (USCAR) have started a project to use of magnesium alloys in motor vehicle. The aim of this project is increasing the usage of magnesium alloys in the motor vehicles to about 100 kilograms in 2020.

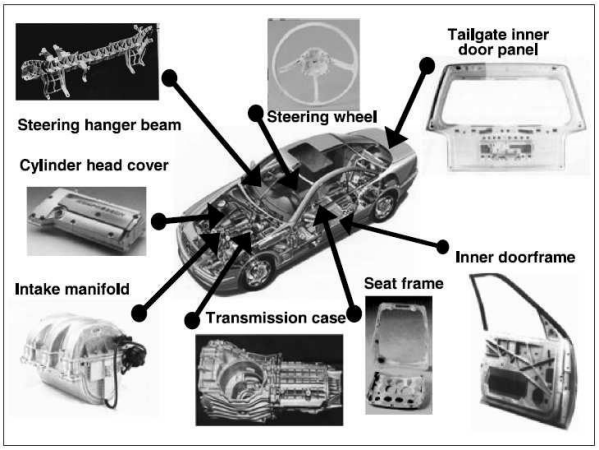

Figure 4.1 Application of Magnesium Alloys in Motor Vehicles [23]

In aerospace industry, some military aircraft contains parts made from magnesium alloys as shown in Figure 4.2 and 4.3. For instance F16, F22, Panavia Tornado have many important parts made from magnesium alloy.

Figure 4.2 TU-95MS: 1550 kg of Magnesium [24]

Figure 4.3 Lockheed F-80C: Complete Magnesium Construction [24]

In Information and Communication Technology (ICT), IBM, HP, Toshiba, Canon and JVC use magnesium alloy in their products. For instance Sony launched two models for Sony mini-disc by using magnesium alloys.

Magnesium alloys are designated according to ASTM B275 (Practice for Codification of Certain Nonferrous Metals and Alloys, Cast and Wrought) which indicates chemical components by weight. The first letter refers to the principal alloying element. The second letter refers to the second most significant alloying element (see Table 4.1 and Figure 4.4). The first number refers to the nominal content of principal alloying element. The second number refers to the nominal content of the second most significant alloying element. The last letter, A or B, differentiates between alloys of similar composition [25]. Chemical composition and mechanical property of AZ91B are given in Table 4.2 and Table 4.3.

Table 4.1 Convention for Alloy Elements Designation [26]

Letter	Alloying Elements
A	Aluminum
C	Copper
E	Rare earth metal
H	Thorium
K	Zirconium
L	Lithium
M	Manganese
Q	Silver
S	Silicon
Y	Yttrium
Z	Zinc

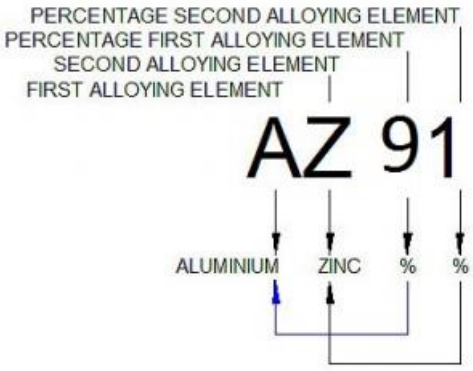

Figure 4.4 Designation Magnesium Alloys [26]

Table 4.2 Chemical Composition of AZ91B (in mass base) [27]

Aluminium, Al	Zinc, Zn	Copper, Cu	Manganese, Mn	Magnesium, Mg
9 %	0.7 %	0.3 %	0.13 %	Remainder

Table 4.3 Mechanical Property of AZ91B [27]

Tensile strength	Yield strength	Poisson's ratio	Elastic modulus	Elongation
230 MPa	150 MPa	0.35	44.8 GPa	3 %

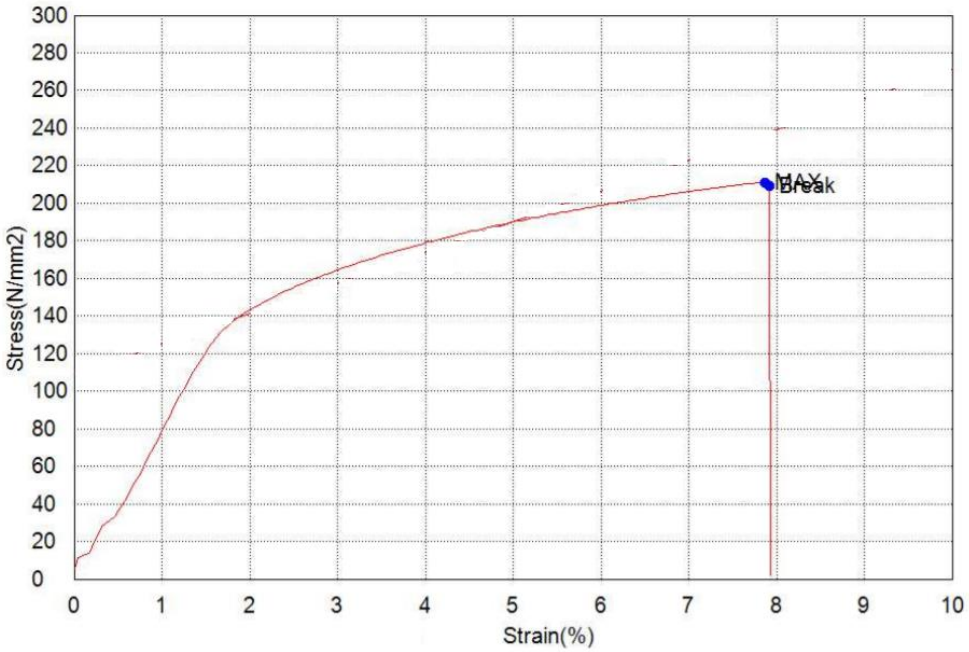

Figure 4.5 Stress-Strain Graph of AZ91B

Crystal structure of AZ91B is one of the important reasons to choose AZ91B as workpiece material. Magnesium alloys have low formability at room temperature because of the hexagonal closed packed crystal structure. This limitation restricts using of magnesium alloys at low temperature, but the searches[28-32] show magnesium alloy exhibits high formability at high temperatures. Enhancement of formability of a material at elevated temperatures can be seen clearly in HCP. Magnesium has nearly ideal axial ratio to choose as a study material. Ideal axial ratio for any crystal structure, is the ratio of the length (or magnitude) of those axes to each other - the longer axis divided by the shorter. The ideal axial ratio is 1.633 for Hexagonal Closed Packed crystal structure [29]. This value is 1.623 for magnesium (at 150º C) [13] .

HCP crystal structure consists of three layers and totally 6 atoms per unit cell. This compacted structure brings high atomic packing factor. Hexagonal closed packed atomic factor is 74% (26% void in unit cell).This ratio is 68% for Body Centred Cubic. Planes and directions are indicated by using 4 coordinate axes (a1, a2, a3 and c).This coordinate system is consist of 3 vectors that has 120º between themselves on a plane and one vector perpendicular to the plane as shown in Figure 4.6.

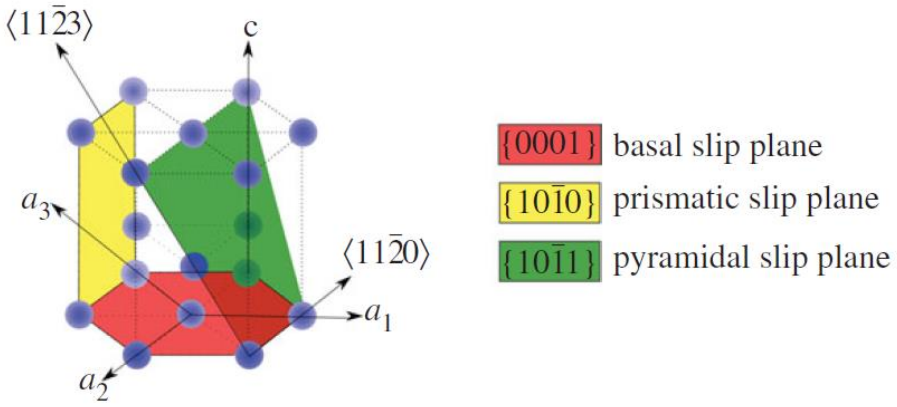

Figure 4.6 HCP Crystal Structure Slipping Planes and Coordinate Axis [30]

Hexagonal Closed Packed crystal structure has 3 three slip planes which are basal slip plane, prismatic slip plane and pyramidal slip plane Due to its hexagonal crystal structure, magnesium has poor ductility at room temperature and complex plastic behavior in the presence of twinning. Magnesium ductility can be significantly improved above about 225 ◦C due to thermal activation of involved additional non-basal slip systems. This has lead to widespread application in the vehicle industry so as to improve fuel efficiency and lower green gas emission. It can be seen that basal, prismatic and first order pyramidal $< a >$ slip systems caused shape change only in the $< a >$ direction. However, an arbitrary deformation is composed of shape changes in both $< a >$ and $< c >$ direction, which can be achieved alone by second order pyramidal $< a + c >$ slip systems. All of the easy $< 11\bar{2}0 >$ slip directions are perpendicular to the c-axis. The slip on the system listed above (except for the second order pyramidal $< a + c >$ slip) does not produce any elongation or shortening parallel to the c-axis. Therefore in order to accommodate the deformation in this direction, there must be a combination of different types of slip systems responsible for arbitrary deformation.

Schmid law states if a crystal is stressed, slip begins when shear stress on a slip system reaches as critical often called as Critical Resolved Shear Stress (CRSS). Schmid factor describes the slip plane and the slip direction of a stressed material, which can resolve the most amount of shear stress.

Ratio of CRSS of basal plane to CRSS of non-basal plane is between about 1:40-1:80 for single crystal models of magnesium alloy [31]. This low CRSS value is attributed low Schmid Factor. On the basal plane Schmid factor is too small due to orientation, so CRSS value on the basal plane is too small compared with non-basal plane. Slipping on the pyramidal slip plane is not expected at room temperature because to activate slipping in the c-axis direction high temperature is required (see Figure 4.7). The CRSS is generally formulated as:

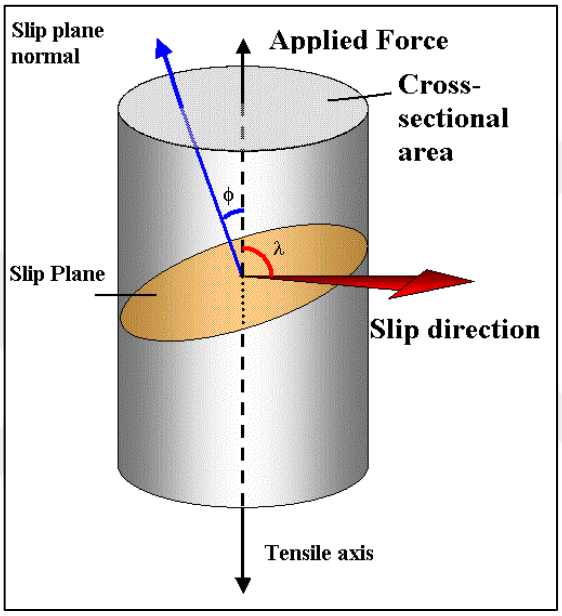

Figure 4.7 Representation of Slip Geometry on the Crystal System [32]

$$\tau_C = \sigma y \cdot cos\phi . cos\lambda \qquad (\mathbf{4.1})$$

Where,

$cos\phi . cos\lambda$ =Schmid Factor

σy=Yield Stress

τ_C=Critical Resolved Shear Stress

4.2.2 1.4003 Stainless Steel

1.4003 stainless steel is designated according to EN10027-2 which indicates chemical composition. The first number, refers to the general structural steel with specified tensile strength is less than 500 MPa. The second number refers to the stainless and heat resisting steels. The third number indicates stainless steel with Nickel < 2.5 % without Molybdenum, Niobium and Titanium. Last two numbers refers to sequence number for stainless steels as shown in Figure 4.8. 1.4003 is named according to European standard, it also designated as 3Cr12, S40977, X2CrNi12 by AISI (American Iron and Steel Institute), UNS (Unified Numbering System) and DIN (Deutsches Institut für Normung) respectively.

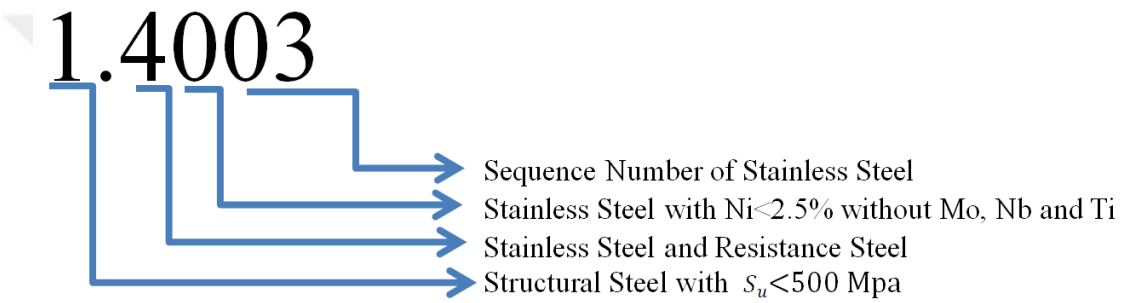

Figure 4.8 Designation of 1.4003 Stainless Steel

Chromium and carbon content have important role with regard to microstructure of 1.4003 ferritic stainless steels. Chromium content in 1.4003 designates directional microstructure, anisotropic tensile property and relatively well developed crystallographic texture. Stainless steel that has less than 18 % chromium content is called as ferritic stainless steel, more than this 18% is called as super ferritic stainless steel [33]. Contents of other elements in ferritic stainless steel have also important role: niobium and titanium prevents precipitation of the harmful chromium carbides, molybdenum enhances corrosion resistance, silica and aluminium increase resistance to oxidation under heat and stabilize ferritic structure [34].

Two of the important microstructural diagrams used for stainless steels are WRC-92 and Schaeffler Delong diagrams.WRC-92 is limited for standard stainless steel composition, so Schaeffler Delong diagram is more popular (see Figure 4.9). Originally, Schaeffler Delong diagram got used for identification of microstructure of weld metal after melting and rapid cooling and this diagram has been found useful

for demonstration of effect of Nickel and Chromium contents on the stabilization of microstructure (ferritic or austenitic).

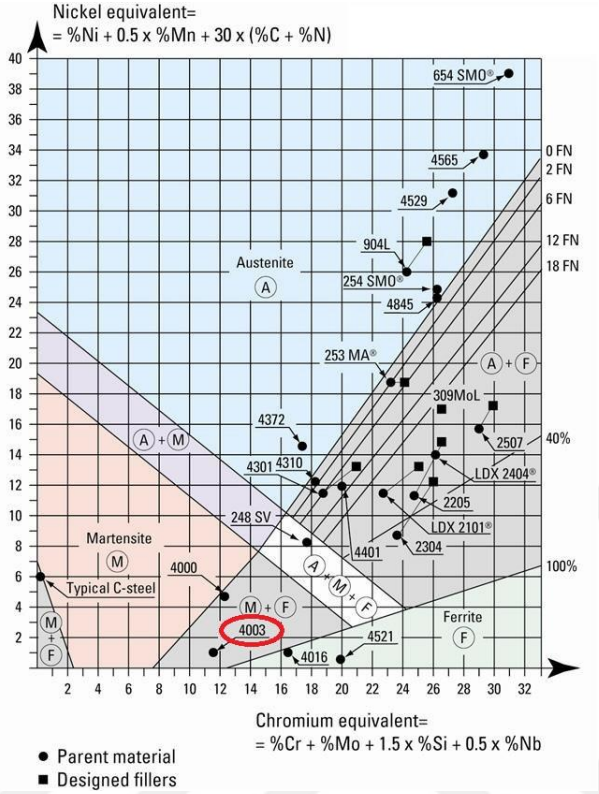

Figure 4.9 Schaeffler Delong Diagram [35]

1.4003 ferritic stainless steel do not present an obvious elastic region as shown in Figure 4.10, there is no exact yield point, so yield point is selected 0.2 % offset tensile yield strength and work hardening is limited. Carbon contents increases strength but chromium content is almost negligible effect on strength.

The mechanical properties and the chemical composition of the 1.4003 stainless steel which is used in this study are determined by using tensile test and spectro-analysis, respectively. The stress-strain curve obtained from the tensile test is shown in Figure 4.10 and the chemical composition is given in Table 4.4. Both of these results are in agreement with the certificate of 1.4003.

Table 4.4 Chemical Composition of 1.4003 Stainless Steel

C	Cr	Mn	Si	P	S	Ni	N	Fe
0-0.03%	10.5-12.5%	0-1.5%	0-1%	0-0.04%	0-0.2%	0.3-1%	0-0.03%	Balance

Tensile test specimen was cut in transverse of rolling direction. Mechanical behaviour of ferritic stainless steel can be widely influenced by alloying elements. 1.4003 is almost insensitive to cold working, this process increases yield and tensile strength in minor degree only and using of 1.4003 at high temperature is not recommended. Subtechnical group of European Commission Research Programme of the Research Fund for Coal and Steel, SAFSS (Structural Applications of Ferritic Stainless Steels), states that 1.4003 has high toughness property at room temperature or below.

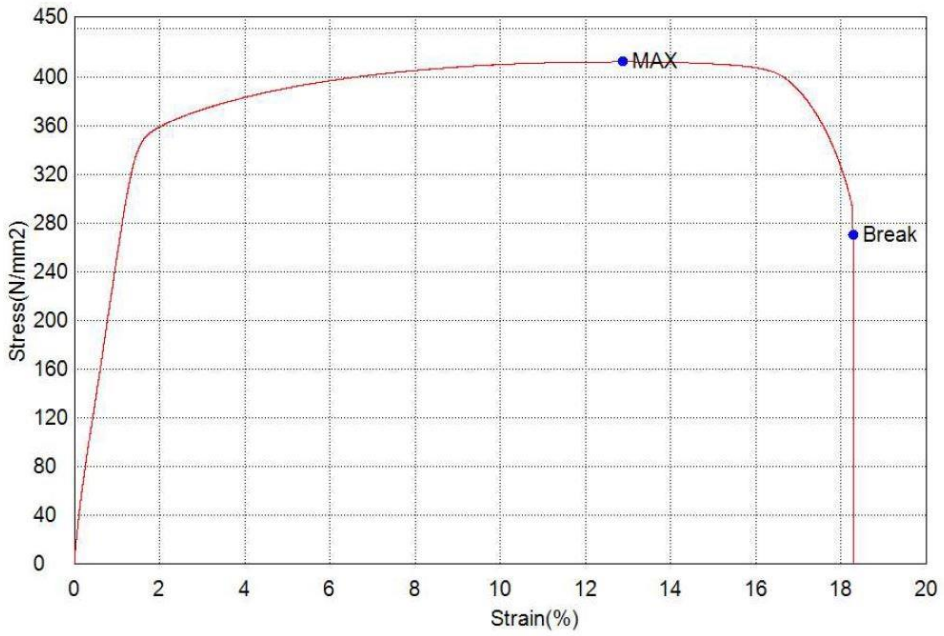

Figure 4.10 Stress-Strain Graph of Specimen (1.4003)

Deformation behaviour of 1.4003 at elevated temperatures: Stress-strain diagram of 1.4003 at different working temperatures are shown in Figure 4.11. Generally, increasing working temperature increases formability of metallic materials. Formability of a material exhibits direct proportion with temperature. The more increase in temperature, the more increasing in formability up to a certain temperature.

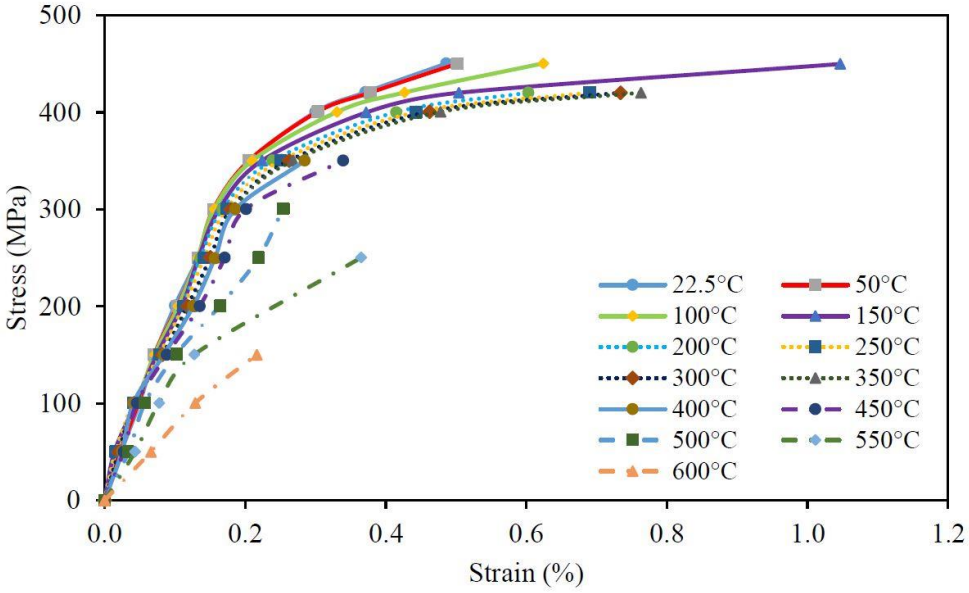

Figure 4.11 Stress-Strain Diagram of 1.4003 for 0.2mm/min Strain Rate at High Temperature Level [36]

The strength reduction factor of 1.4003 stainless steel is derived from tension test [1] which is shown in Figure 4.12. Changing in strength reduction factor at 600ºC can be observed clearly, for this reason formability test in this study is conducted at 600ºC.

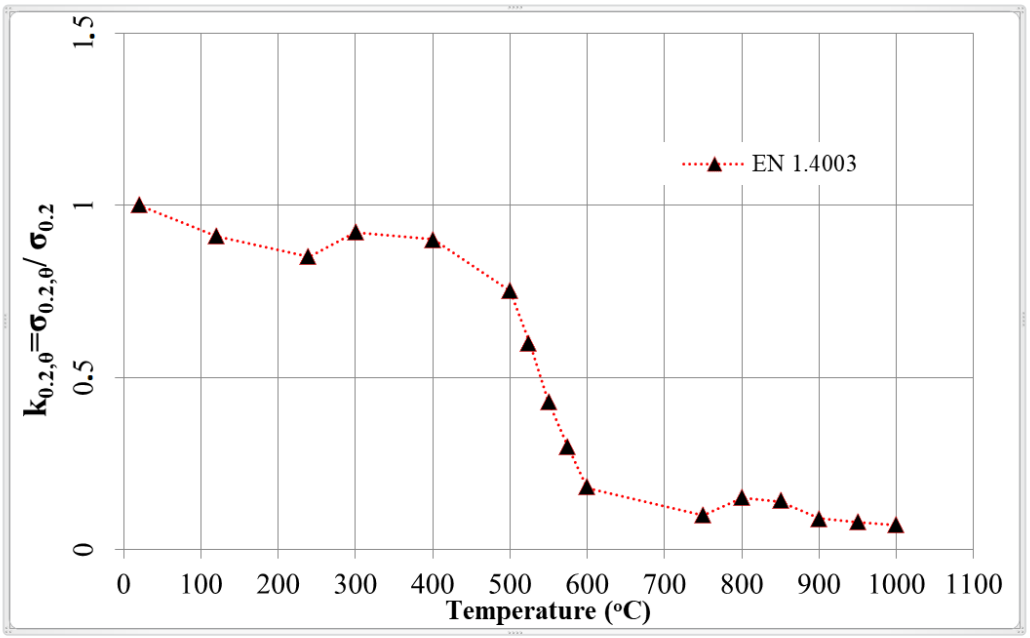

Figure 4.12 Changing Yield Strength of 1.4003 Stainless Steel with respect to Temperature [1]

4.3 Experimental Procedure

4.3.1 Die Set

In this study V- bending die was used for experimental work. The photograph and the schematically representation of the V-bending die are illustrated in Figure 4.12 and Figure 4.13, respectively.

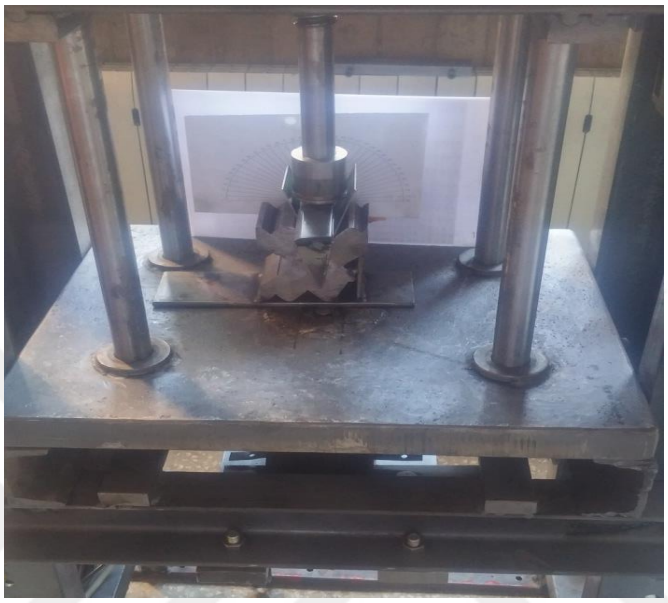

Figure 4.13 Die Set

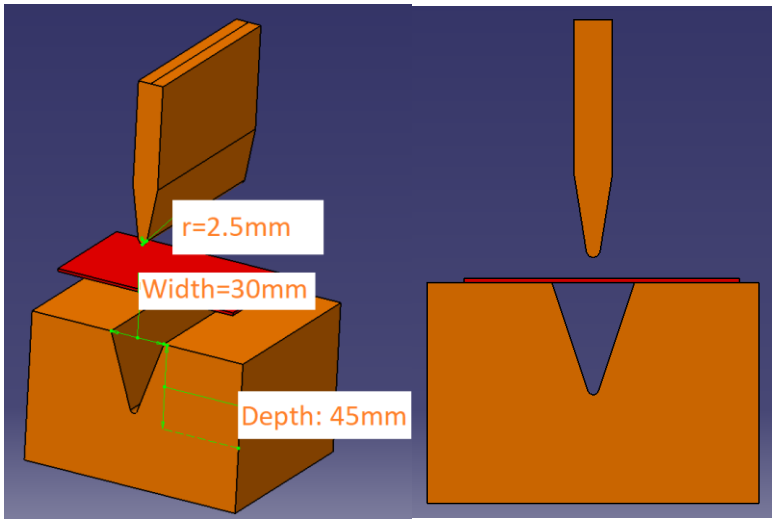

Figure 4.14 Illustration of V-Bending

Ease of manufacture and observability of degree of bending are some of the reasons why V-bending is used.

4.3.2 Servo Press and Induction Unit

In this study bending tests were conducted by using servo controlled press machine. The press has maximum capacity of 2000 kg and it is shown in Figure 4.14. Ratio of servo motor pulley diameter to power screw pulley diameter is 3. The loads were measured by using load cell of type Keli LFSC-A 50 kN capacity.

Figure 4.15 Servo Controlled Press Machine and Induction Unit

In this study is RT-380M50 which was manufactured by RETERM was used. Technical properties of induction heating unit was given in Table 4.6

Table 4.5 Technical Properties of the Induction Heating Unit

Model	RT-380M50
Technical Property	
Machine Dimensions (mm)	515x631x566
Power (KW)	50
Capacity (Kg/h)	75
Voltage (Volt)	380
Current (Amper)	100
Frequency Range (KHz)	1.7-12
Cooling Water Pressure (bar)	3-6
Coil Diameter (mm)	8

4.3.3 Specimen Preparation and Heating

Firstly AZ91B specimens were cut as rectangular dimension (60 mm x 170 mm x 1.5 mm). The specimens were bent with different bend angles (40°, 60°, 75° and 90°) at 10 mm/sec by the servo press. The specimens were heated up to 180℃ by resistance heating. Level of temperature was measured by infrared heat measurement device during heating process. Heated specimens was placed onto die and bent at 150℃. Changing colour of film layer was observed because of heating.

The 5 mm thick specimens cut from 1.4003 stainless steel sheet plate. The specimens cut to required dimension (60 mm x 100 mm x 5 mm) by laser cutting machine. Workpiece were placed into V-bending die and pressed. The specimens were heated up to 570℃. During bending operation due to slipping grain heat occurs, this heat increases temperature up to 600℃. The reason of choosing the 600℃ for forming temperature is the reduction of yield strength at this temperature (see Figure.4.12)

4.3.4 Bending Test

After preparation of specimens for both cold and locally heated, these specimens were placed onto die. Punch pressed the specimens with a rate of 10 mm/sec via servo press. To obtain desired angles, required stroke values were input to servo press control unit.

CHAPTER 5

FINITE ELEMENT MODELLING

5.1 Introduction

In this chapter, general procedure of finite element modelling and the running steps of DEFORM-2D package are presented. The definition of material model and boundary conditions are described.

5.2 FEM in Sheet Metal Forming

Simulation is more economical than real applications in most of the time. FEM for sheet metal forming has been developed in recent years; there are a lot of FEM packages for only sheet metal deformation. Sheet metal forming is a process of shaping thin sheets of metal by applying pressure through male or female dies or both. In most of used sheet-formatting processes the metal is subjected to primarily tensile or compressive stresses or both. During the last three decades considerable advances have been made in the applications of numerical techniques, especially the finite element methods. These methods are useful because one can use them to find out facts or study the processes in a way that no other tool can accomplish. The properties of many materials are available in the material database of the FE package but if it is not available, it can be defined by user. There are critical points to take into consideration for FEM;

- Physical definition of problem should be correct.
- Idealizations, assumptions and neglecting should satisfy the previous studies.
- Mesh types and density should be proper for process.

- Boundary condition should be same with real application (friction, heat transfer coefficient…)
- Correct material laws and parameter must be used (isotropy, anisotropy, failure type).
- Correct numerical parameter should be selected (damage factor, remeshing criteria).

5.3 Finite Element Procedure and Modelling

Finite element modelling is important in terms of observation of behaviour of model after certain process. Mostly, finite element modelling is one of the cheapest methods to predict result of operations. It is also useful to reduce time consumed for process design. In some cases, it is impossible to determine forming loads and encountered tool stresses analytically, because of shape complexity. Therefore, finite element modelling is preferred for solving of real complex problem in a short period of time. Main steps of FEM packages are shown in Figure 5.1.

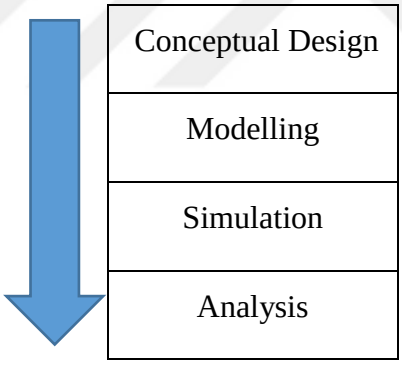

Figure 5.1 Main Steps of FEM Packages

In this study DEFORM-2D is used for finite element modelling. Deform^{TM} 2D is one of the most popular software for sheet metal forming. Deform^{TM} 2D is based on three main section. These are Pre-Processor, Simulation Engine and Post-Processor. Display capture of Deform^{TM} 2D is shown in Figure 5.2.

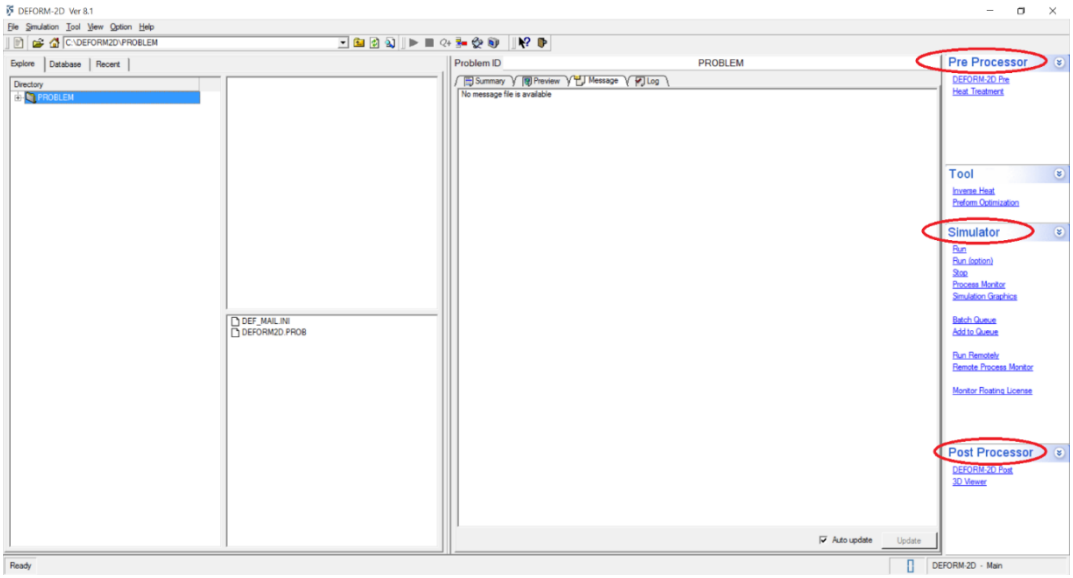

Figure 5.2 Display Image of Deform™ 2D

Pre-Processor: In this section (as shown in Figure 5.3) material of objects, behaviour of material, temperature of object, geometry of objects mesh type and frequency, movement of objects, boundary condition of objects and nodal property of objects can be defined.

Simulation Engine: is used for running modelled system. Steps can be seen in summary window is shown in Figure 5.4.

Post-Processor: It is the final step of Deform™ 2D program (see in Figure 5.5). Results obtained during running process (damage, displacement, strain, strain rate, stress, velocity, temperature) can be seen in this section. Behaviour of any points on objects during simulation also can be detected.

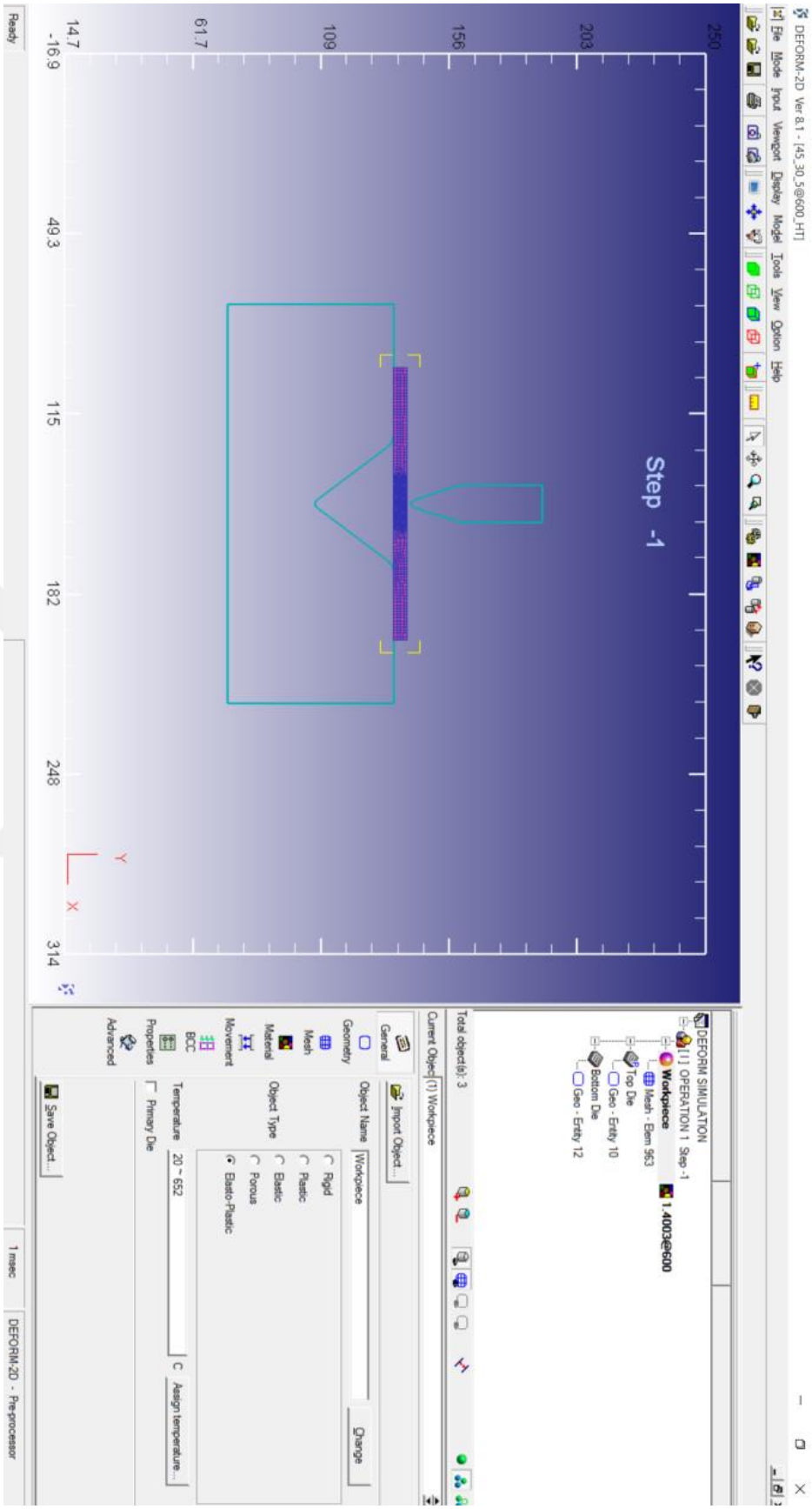

Figure 5.3 Pre-Processor Window of Deform™ 2D

Figure 5.4 Running Window of Deform™ 2D

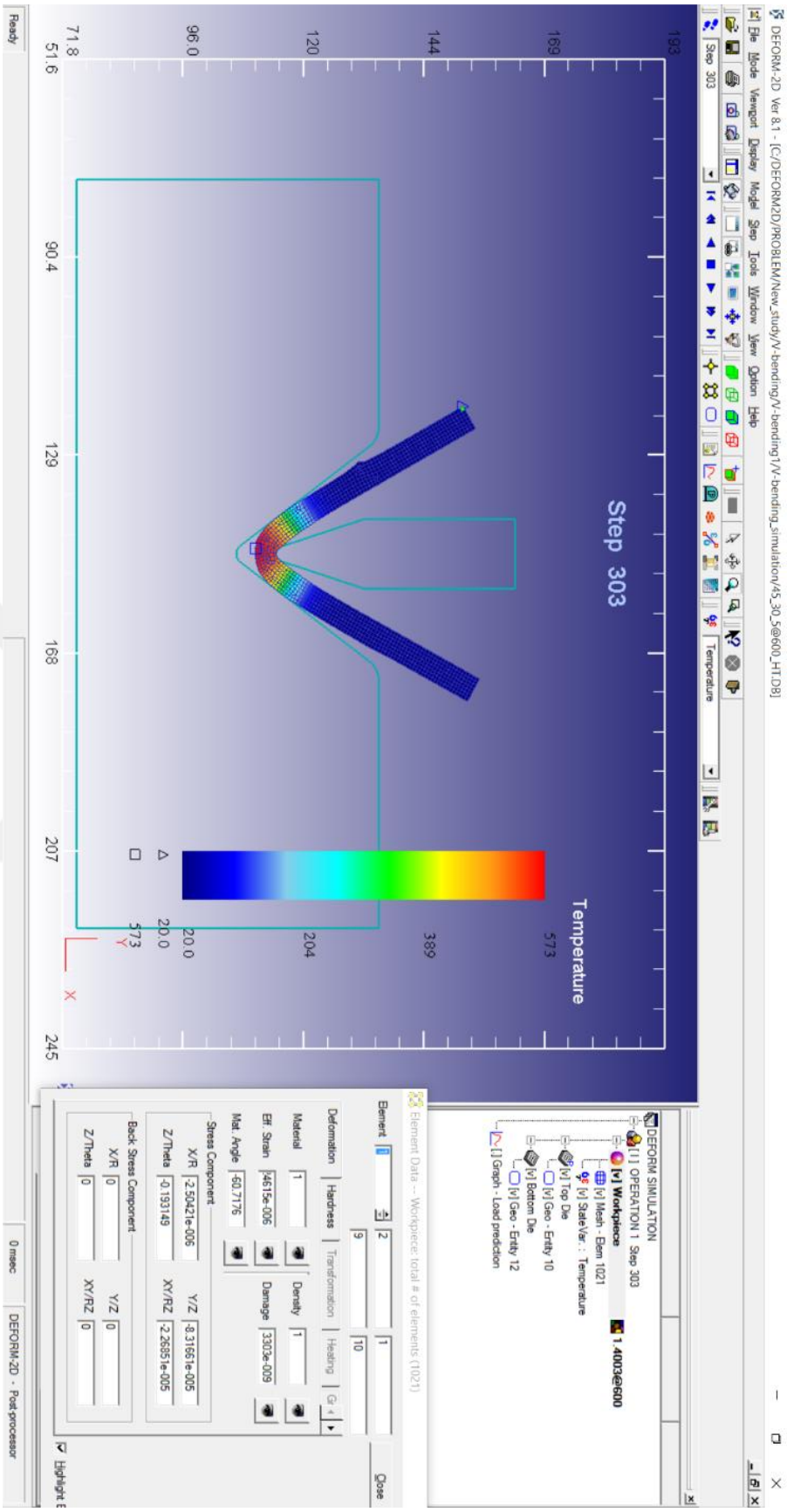

Figure 5.5 Post-Processor Window of Deform™ 2D

In this study, upper die and bottom die were taken as rigid bodies and the workpiece was defined as elastoplastic material. The rigid-elastoplastic modelling reduces simulation time by defining interface contact elements easily. This is a general route in Deform^{TM} 2D for metal forming problems. If tool stresses are needed, a subsequent run must be carried out by transferring interface loads on die components.

Owing to providing realistic results in terms of springback and thermal property, workpiece materials were selected as elastoplastic material type. Mechanical properties of AZ91B and 1.4003 were not available in Deform^{TM} 2D default database, so required mechanical properties for this study was input the database. Flow stress-strain curves for AZ91B and 1.4003 was shown in Figure 5.6 and 5.7.

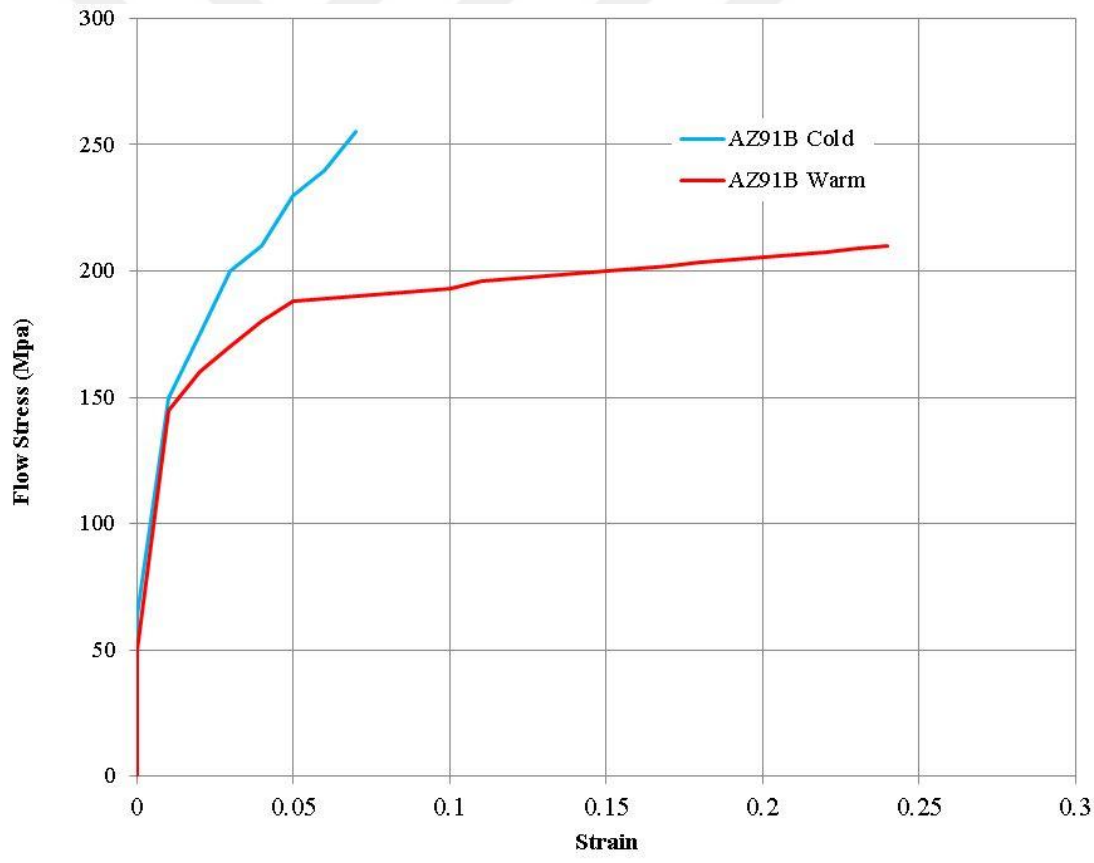

Figure 5.6 Flow Stress - Strain Curves for AZ91B Cold (25^0C) and Warm (150^0C) for 0.2 mm/min Strain Rate

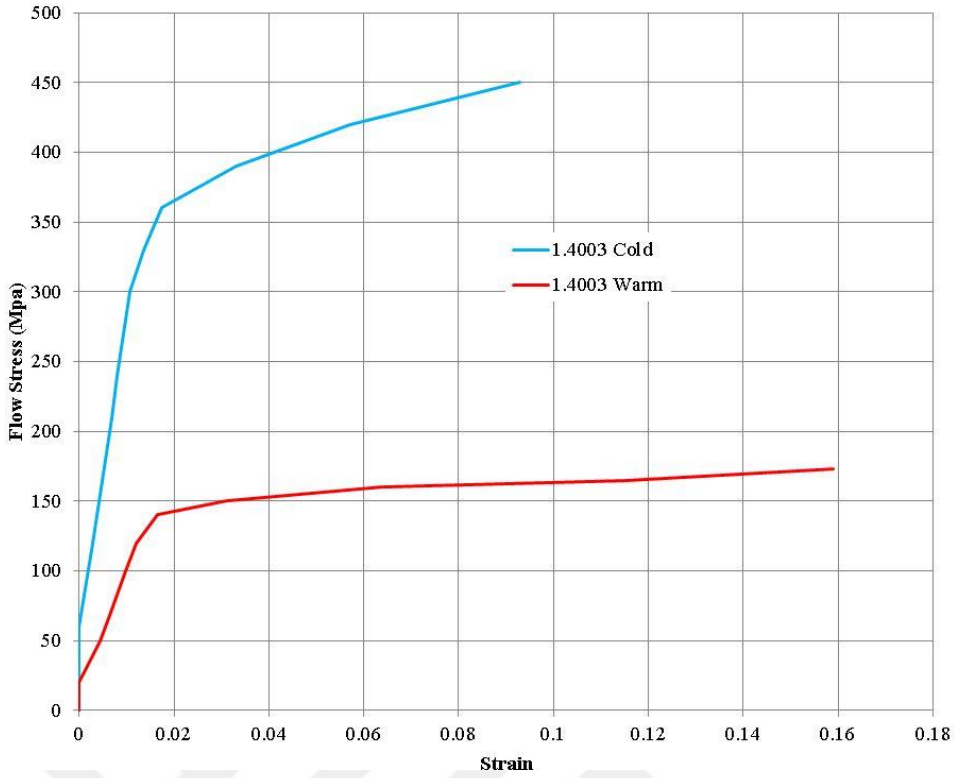

Figure 5.7 Flow Stress - Strain Curves for 1.4003 Cold (25^0C) and Warm (600^0C) for 0.2 mm/min Strain Rate

Ductility of metallic materials is generally defined as the ability to deform plastically without fracture. It is usually expressed as a measure of the strain at fracture in a tension test. However the percentage elongation in a tensile test is often dominated by the uniform elongation, which is dependent on the slope of the stress-strain curve. The end of uniform elongation coincides with the onset of plastic instability. It appears that the elongation value is too complex to be regarded as a fundamental property of a material and seems reasonable to assume that any criterion of fracture will be based on some combination of stress and strain rather than on either of these quantities separately. In this study Normalized Cockroft-Latham is used as fracture criterion[37] . This fracture criterion is expressed with following formulation:

$$\int_0^{\varepsilon_f} \frac{\sigma_{max}}{\sigma_E} d\varepsilon_{pl} = C \qquad (\mathbf{5.1})$$

where

σ_{max} = The maximum principle stress ε_f = The limit fracture strain

ε_{pl} = The plastic strain σ_E = The effective stress

The critical damage factor can be obtained by using tensile test. The damage factors of AZ91B were obtained as 0.12 and 0.84 for 25^{o}C and 150^{o}C, respectively. The damage factors of 1.4003 stainless steel were obtained as 0.35 and 1.8 for 25^{o}C and 600^{o}C, respectively. Cracks begin when the damage value of workpiece reaches to its critical value. In the finite element model, the crack is shown by element deletion.

Deform package can be used for axisymmetric, plane strain and torsion modelling. According to workpiece geometry this condition is selected from in simulation control window of Pre-Processor section in Figure 5.8. The bending process modelled in this study is considered as plane strain problem due to high width to thickness ratio.

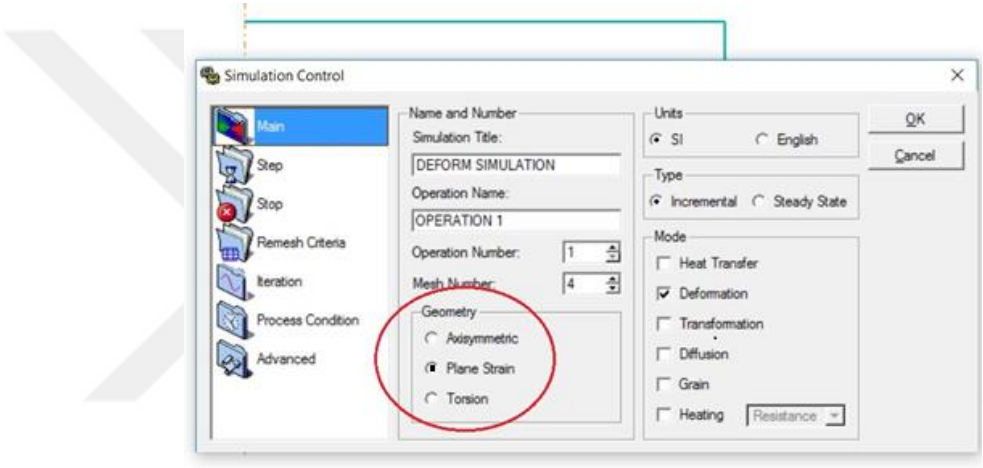

Figure 5.8 Simulation Control Window

Also, friction types and values are other parameters for metal forming process. The friction values were defined between the workpiece and the bottom die, and the workpiece and the punch. The friction type was selected as Coulomb's model and the values were determined from ring compression tests. Table 5.1 shows the friction values for each type of models.

Table 5.1 Friction Values

TYPES	AZ91B		1.4003 Stainless Steel	
	Cold	Warm	Cold	Warm
Workpiece-Bottom Die	0.14	0.33	0.12	0.3
Workpiece-Punch	0.14	0.33	0.12	0.3

Mesh and node number must be defined to any FE package. Mesh type is quadrilateral for Deform FEM programme. AMG (Automatic Mesh Generator) is a tool of DEFORM and it is used to solve the problems in large deformation and to provide an optimized re-meshing capability. The Newton-Rapson Method and the Langrangian incremental type were used for iteration method and the solver, respectively. The number of elements and nodes used in the models are shown in Table 5.2.

Table 5.2 Elements and Nodes Numbers

TYPE	AZ91B Cold & Warm			
	Elements	Nodes	Elements	Nodes
Workpiece	2971	3430	2971	3430
	1.4003 Cold & Warm			
	Elements	Nodes	Elements	Nodes
Workpiece	1566	1715	1566	1715

CHAPTER 6

RESULTS AND DISCUSSION

6.1 Experimental and Finite Element Results for AZ91B Bending

The specimens made from AZ91B were bent for different angles ($45^0, 60°, 75°$ and 90°) by using die described in chapter 4. The bending tests were carried out as cold and locally heated condition.

Firstly cold bending was conducted up to 90° inside bending angle, as shown in Figure 6.1.

Figure 6.1 Cold Bent Specimens with Angle of 90°

No crack was observed at 90° cold bending, because minimum condition to cracking was not satisfied in terms of formability. Some scratches were observed on contact

region of specimen and punch due to pressing. The results of FEM simulation are in well agreement with experimental one as shown in Figure 6.2.

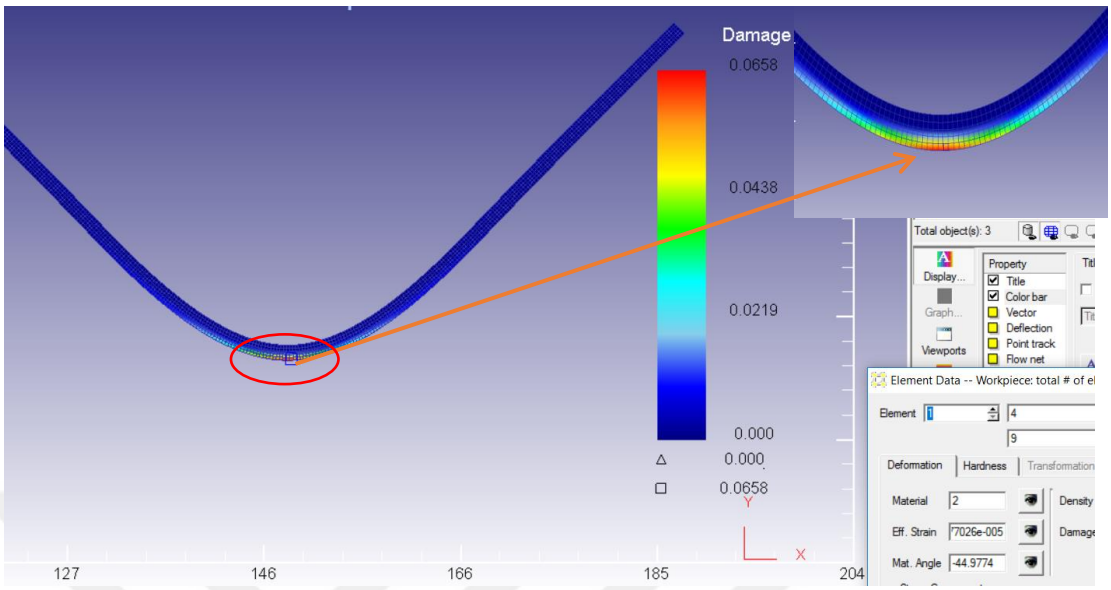

Figure 6.2 Cold Bent Specimen with Angle of 90° in Deform™ 2D.

Secondly, cold bending was carried out with an angle of 75° which is shown in Figure 6.3. Crack was not observed for this angle in experiment.

Figure 6.3 Cold Bent Specimen with Angle of 75°

Figure 6.4 shows the FEA for cold bent specimen with angle of 75° and damage factor did not reach to the critical value for cold forming of AZ91B.

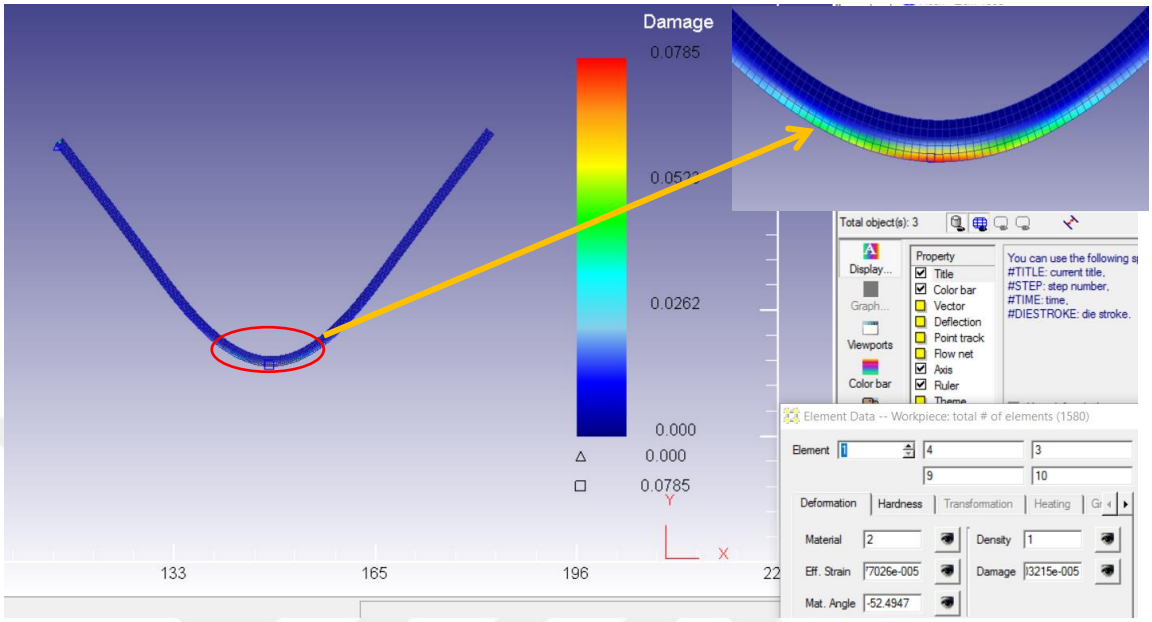

Figure 6.4 Cold Bent Specimen with Angle of 75° in Deform™ 2D.

Thirdly, cold bending was conducted for bend angle of 60°, as shown in Figure 6.5. Cracks were observed at bend angle of 60° for cold bending process.

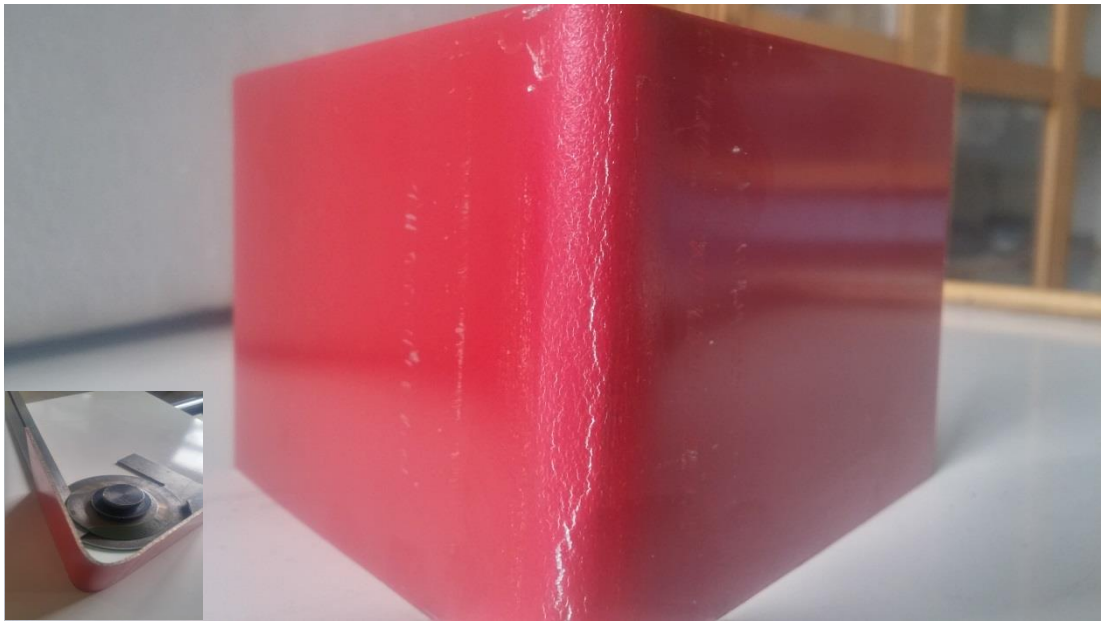

Figure 6.5 Cold Bent Specimen with Angle of 60°

Finite element analysis results were in good agreement with the experimental results for this angle. The damage factor for this bending (0.124) condition was higher than the critical damage factor value (0.12). Because of this reason, cracks started which is shown in Figure 6.6.

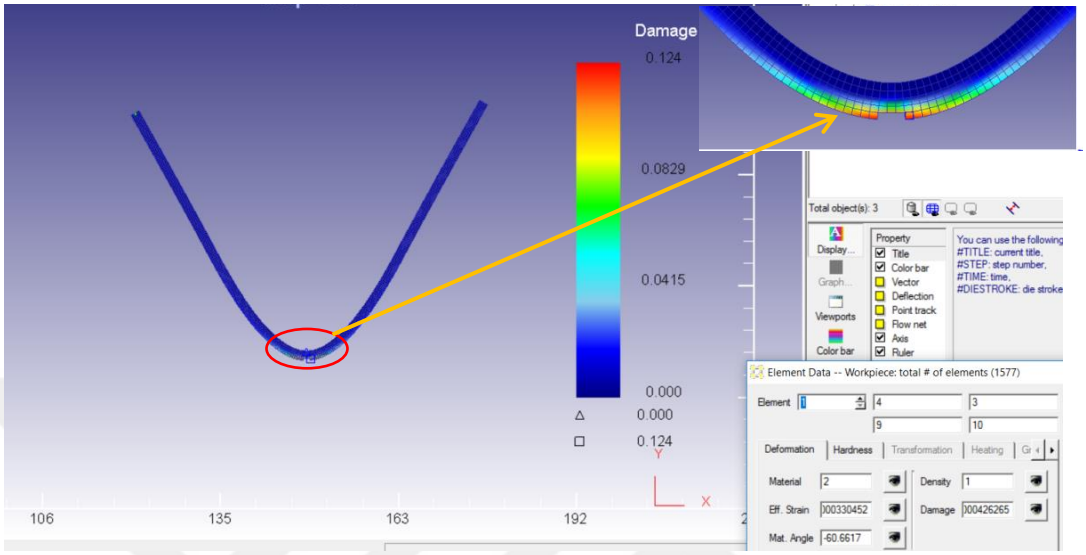

Figure 6.6 Cold Bent Specimen with Angle of 60° in Deform™ 2D.

Fracture can be seen clearly at 45° experimentally cold bending as illustrated in Figure 6.7.

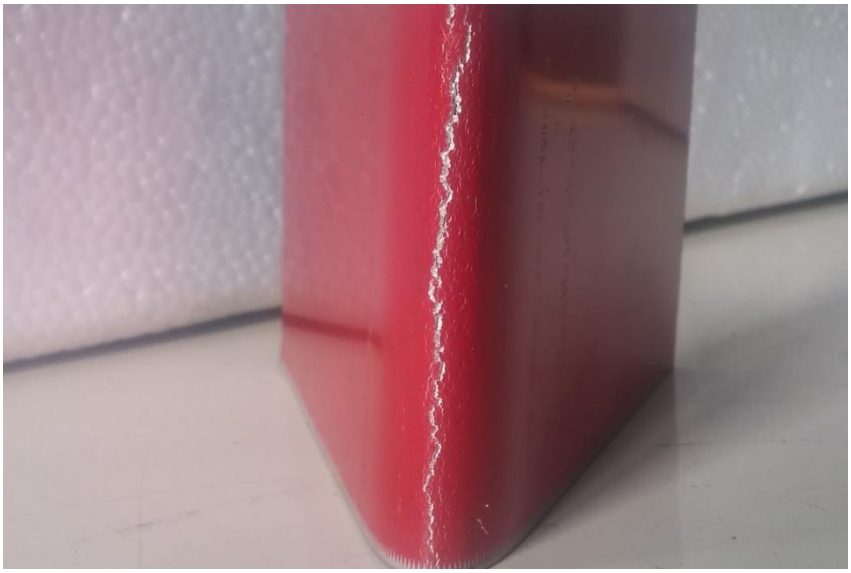

Figure 6.7 Cold Bent Specimen with Angle of 45°

Finite element method results are in good agreement with experimental results for angle of 45°. It is observed that cracks can be seen obviously bend angle of 45° for cold bending as shown in Figure 6.8.

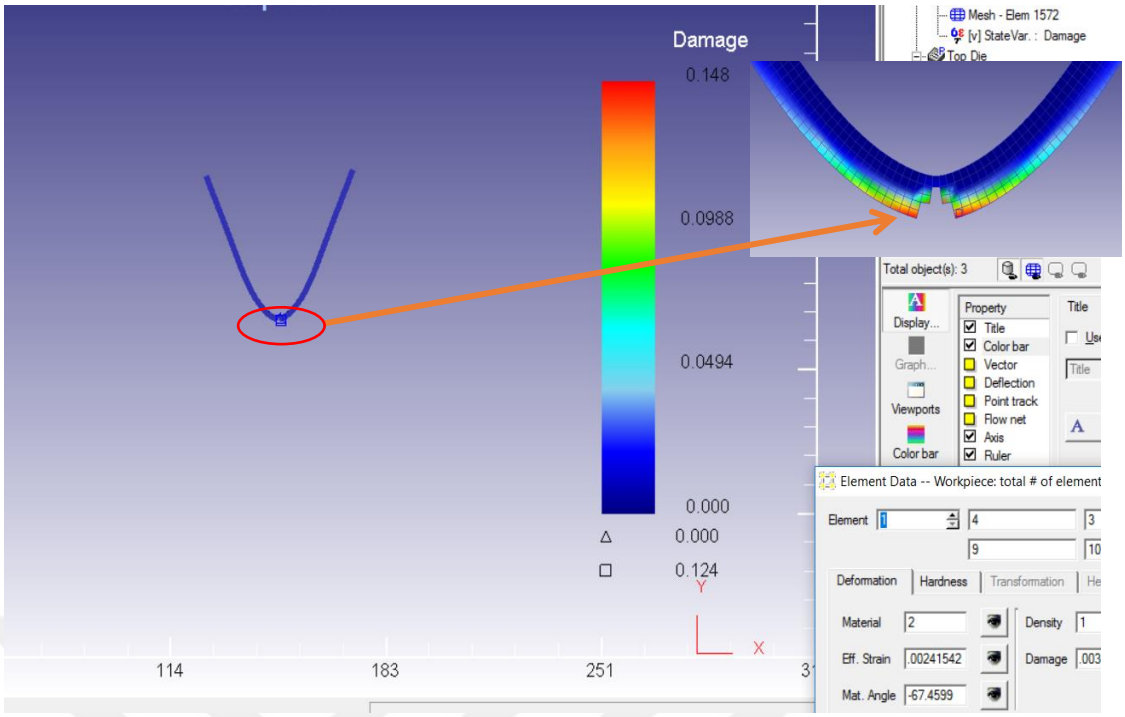

Figure 6.8 Cold Bent Specimen with Angle of 45° in Deform™ 2D.

Crack conditon of cold bending for AZ91B was shown in Table 6.1.

Table 6.1 Summary of Cold Bending for AZ91B

Temperature	Bend Angle	Crack for Experimental	Crack for FEM	Damage Factor in FEM
Room	90	No	No	0.065
Room	75	No	No	0.078
Room	60	Yes	Yes	0.124
Room	45	Yes	Yes	0.148

Load-stroke diagram for experimental results of AZ91B was shown in Figure 6.9. The load stroke diagram obtained from FE simulation was superimposed in Figure 6.9. The maximum difference between load values obtained from experimental study and FEM is 9.2 %. This differences may come from lubrication condition.

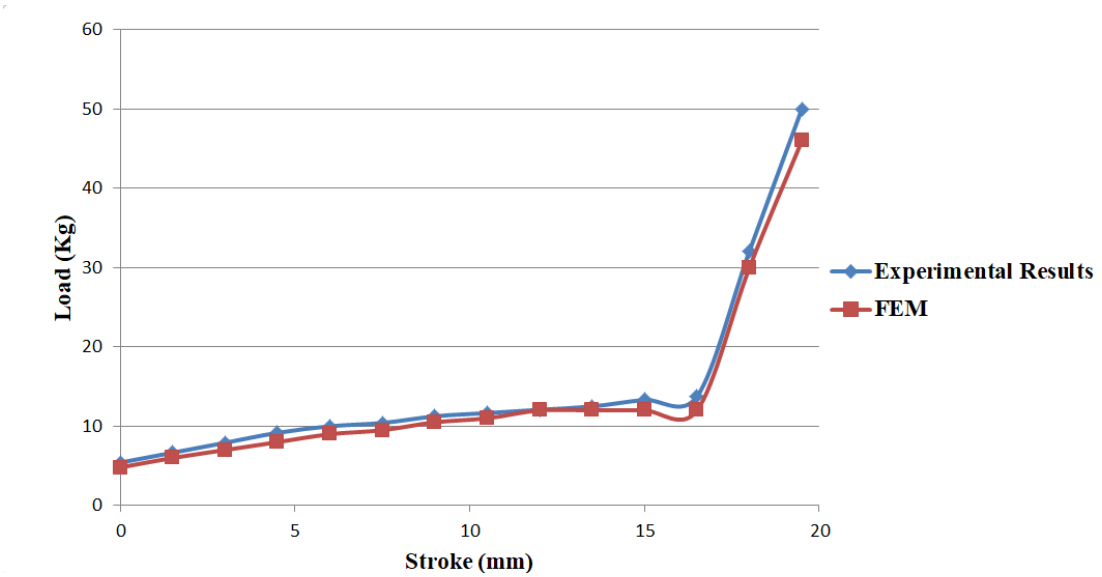

Figure 6.9 Load-Stroke Diagram of Cold Bending of AZ91B

Minimum bend radius (R_{min}) is related to reduction in area in tension test (r) and thickness (t). Recommended minimum bend radius for magnesium at room temperature is [20]:

t=1,5mm and $r = 8$, $$R_{min} = 5t = 5.(1{,}5) = 7{,}5\ mm \qquad (\mathbf{5.1})$$

or, more accurately $$R_{min} = t\left(\frac{50}{r} - 1\right) = 1.5\left(\frac{50}{8} - 1\right) = 7.875\ mm \qquad (\mathbf{5.2})$$

where r is reduction in area and it is determined for magnesium alloys as 8% [38]. Inside radius of workpiece was measured as 6 mm (see Figure 6.10). First cracks were observed at angle of 60° when cold bending because of minimum inside bend radius reduced below minimum bend radius value (R_{min}) .

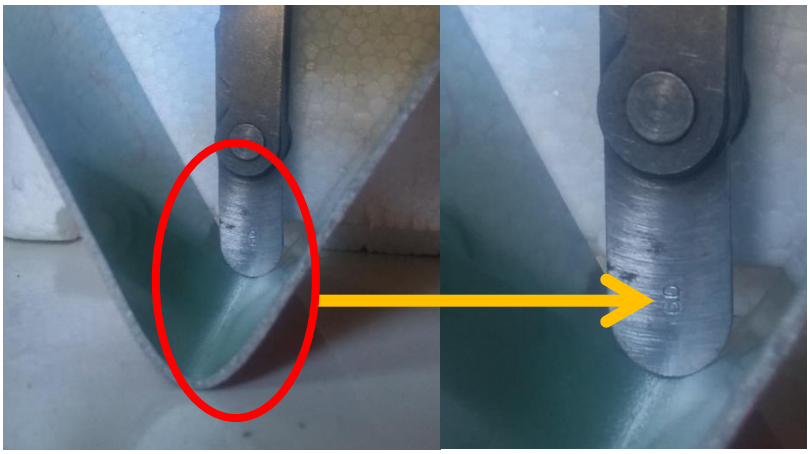

Figure 6.10 Measuring of Radius of Cold Bent AZ91B

After cold bending process for AZ91B, specimens were locally heated and bent experimentally and FEM was simulated for locally heated specimens as shown in Figure 6.11.

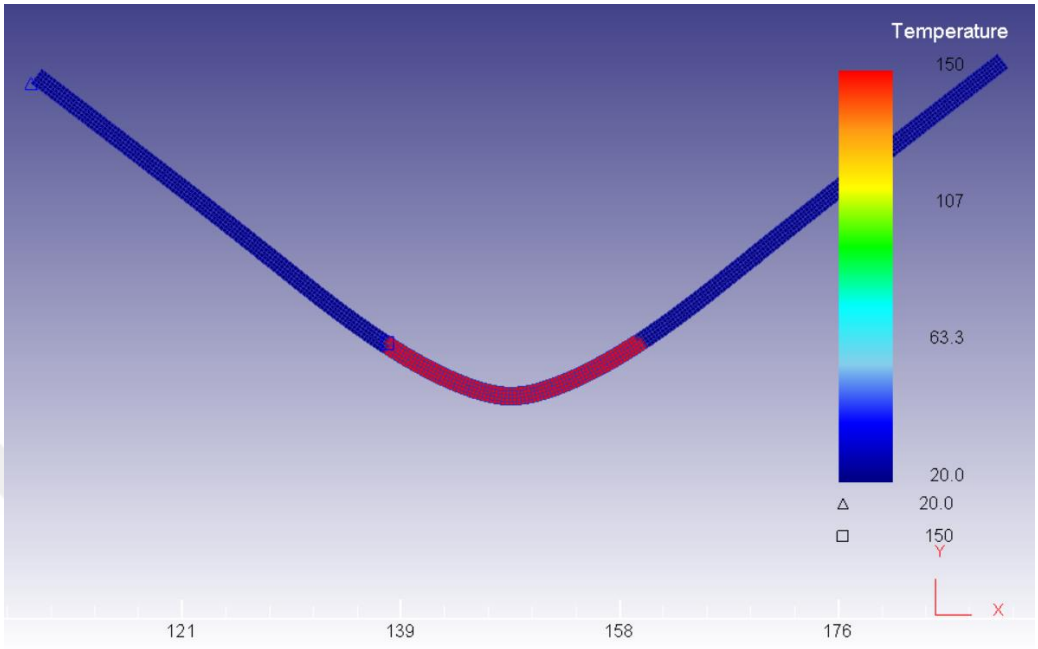

Figure 6.11 Locally Heated Specimen

Firstly specimen was heated up to 180℃ by resistance heating and bent angle of 90° experimentally as shown in Figure 6.12. The crack formation was not observed. Colour changing was seen because surface paint of sheet burnt out as illustrated in Figure 6.13. In finite element model, damage factor did not reach the maximum, so it was in good agreement with experimental study.

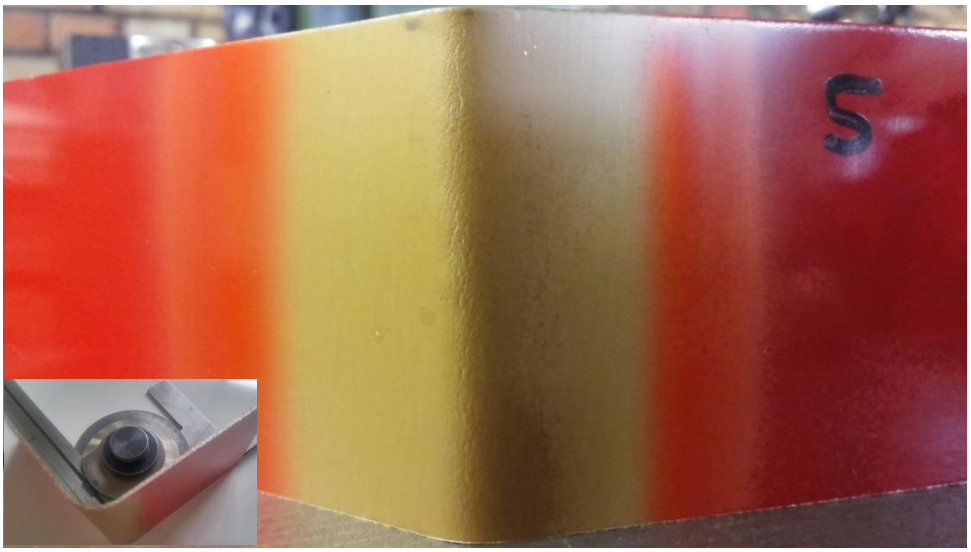

Figure 6.12 Locally Heated Bent Specimen with Angle of 90°

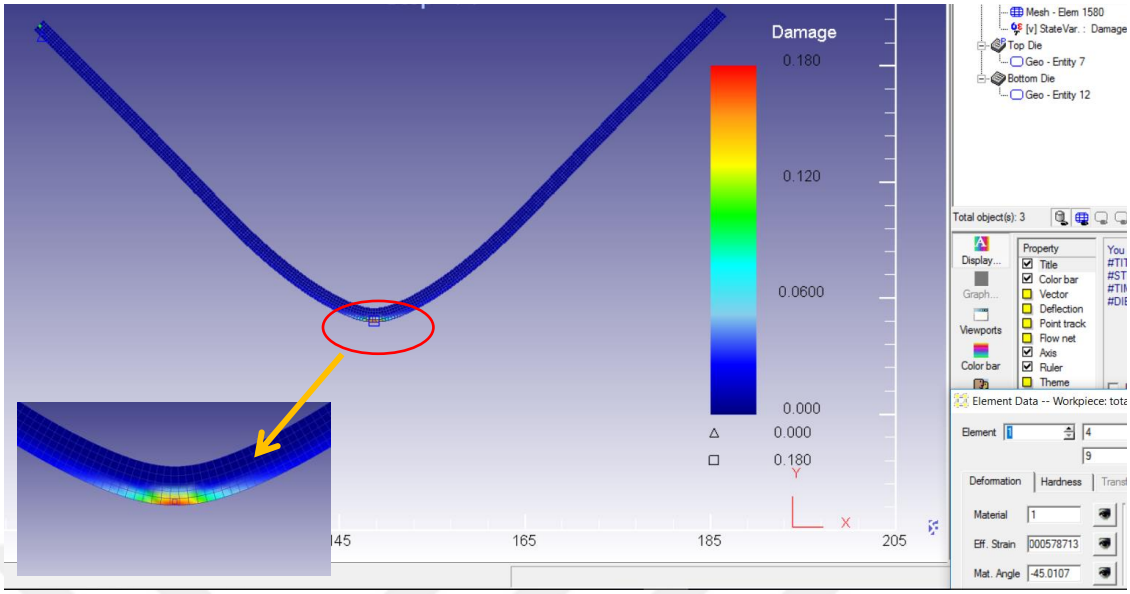

Figure 6.13 Locally Heated Bent Specimen with Angle of 90° in Deform™ 2D.

Specimen was bent angle of 75° by using locally heating, Figure 6.14 shows the still there was no crack on the outer side of bending area of specimen. This condition was in good agreement with FE results as shown in Figure 6.15.

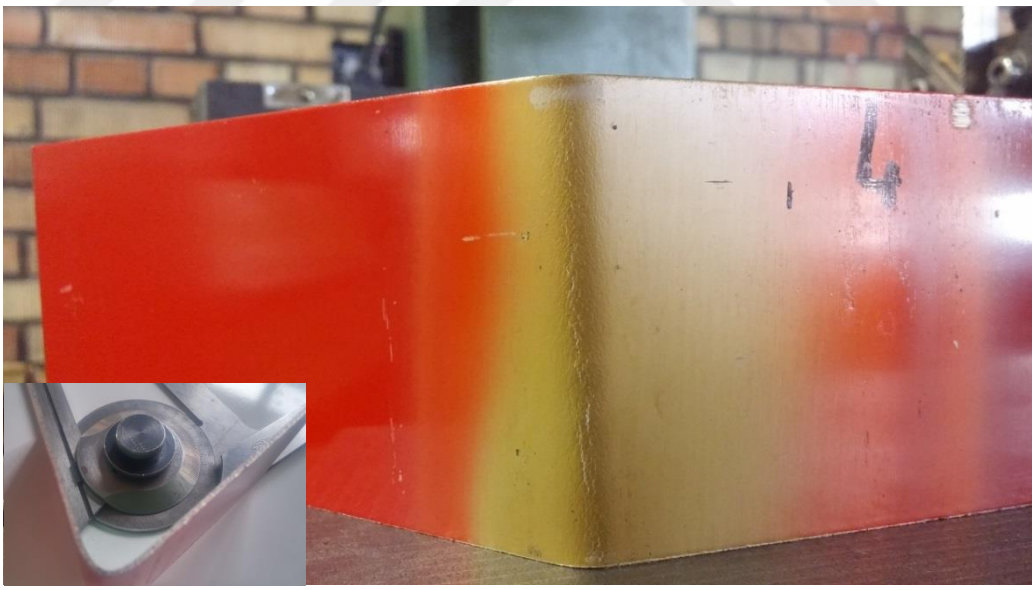

Figure 6.14 Locally Heated Bent Specimen with Angle of 75°

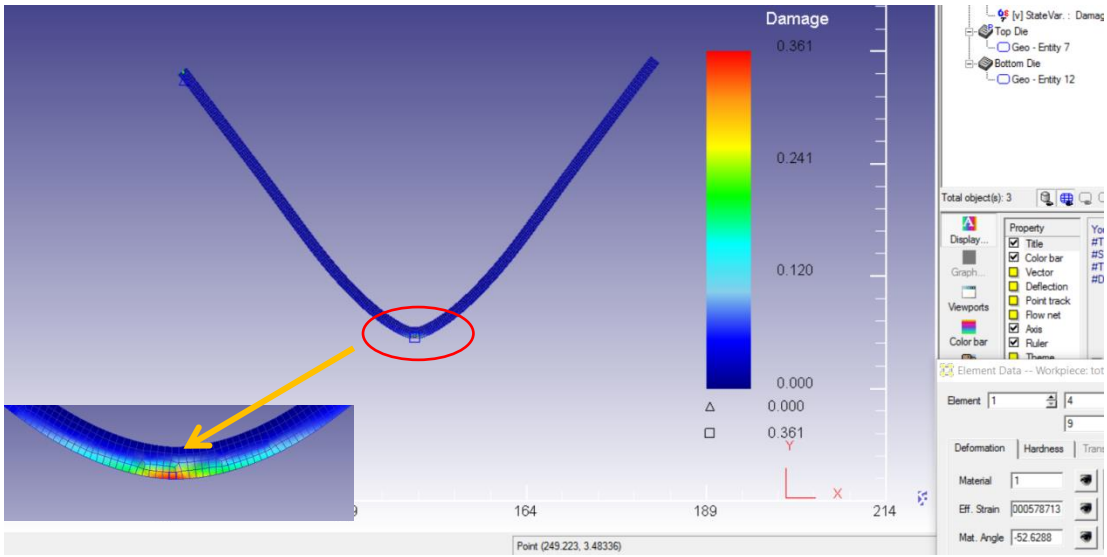

Figure 6.15 Locally Heated Bent Specimen with Angle of 75° in Deform™ 2D.

Then 60° bend angle was applied the specimen as shown in Figure 6.16 and Figure 6.17. Crack formation was not observed, the cracks on the surface is on the surface paint.

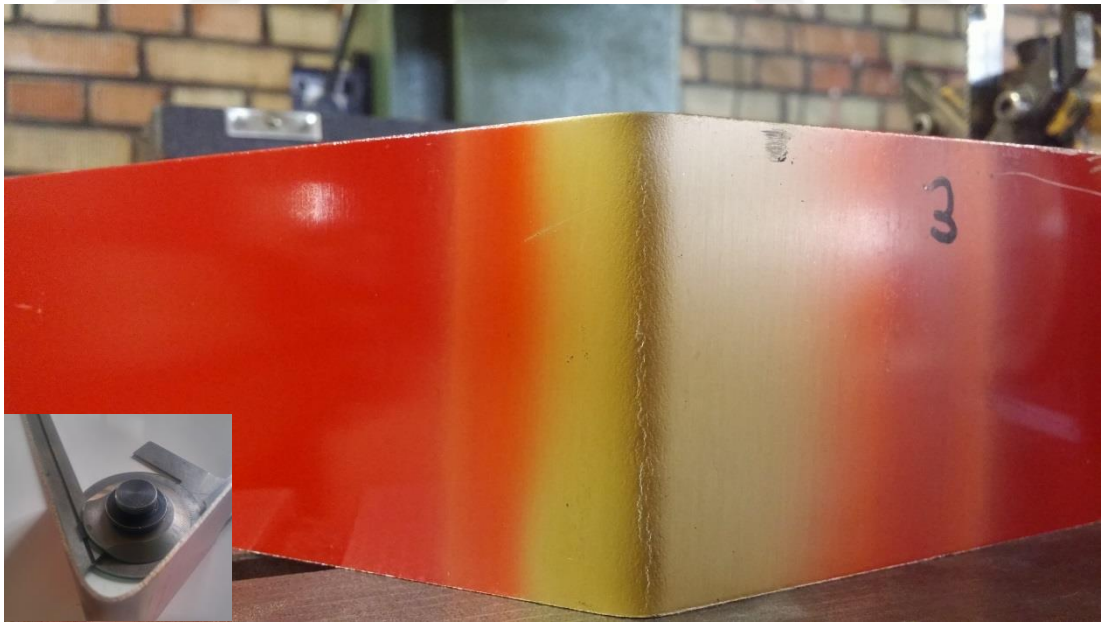

Figure 6.16 Locally Heated Bent Specimen with Angle of 60°

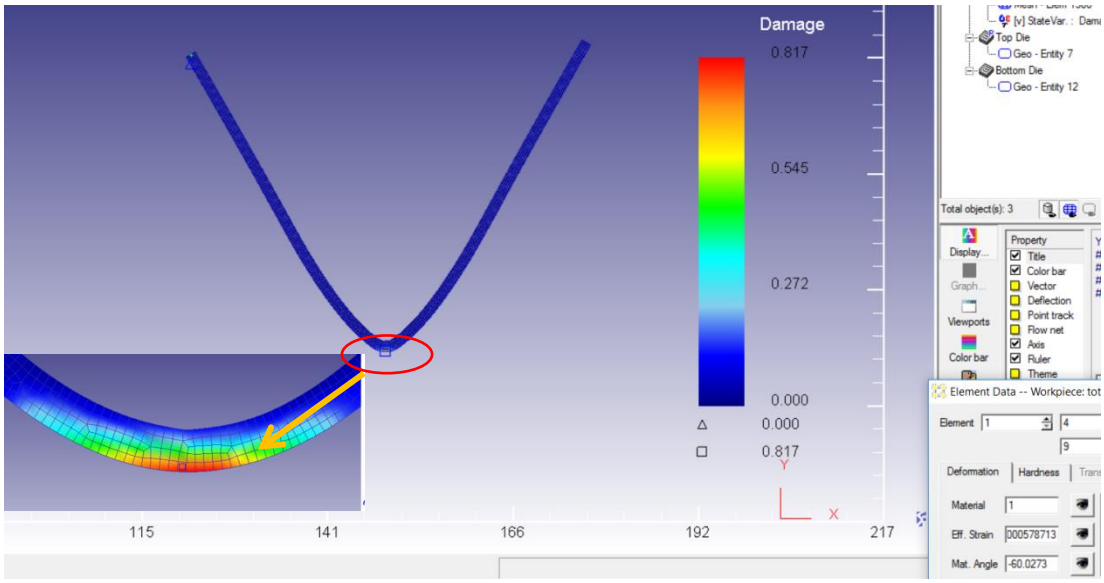

Figure 6.17 Locally Heated Bent Specimen with Angle of 60° in Deform™ 2D.

When specimen bent with an angle of 45°, cracks can be seen as shown in Figure 6.18. FEM result is also verified the experimental results in Figure 6.19.

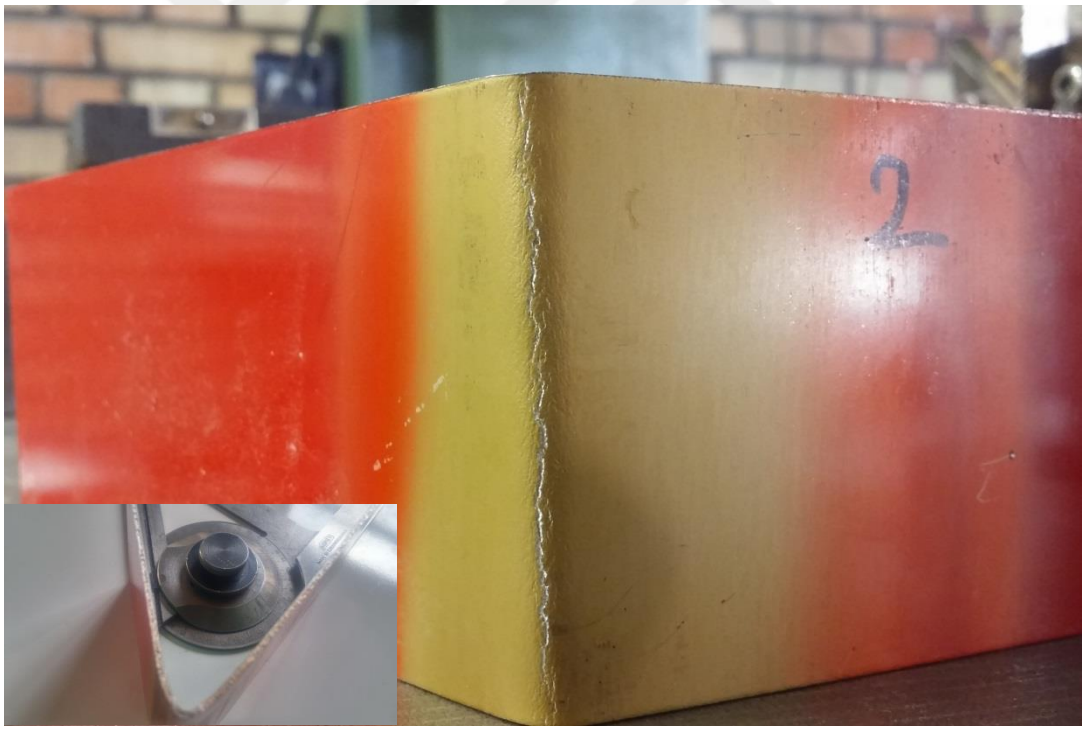

Figure 6.18 Locally Heated Bent Specimen with Angle of 45°

Cracks were not observed in locally heated bending operation for bend angle of 45° due to increasing of flow stress of workpiece on bending area.

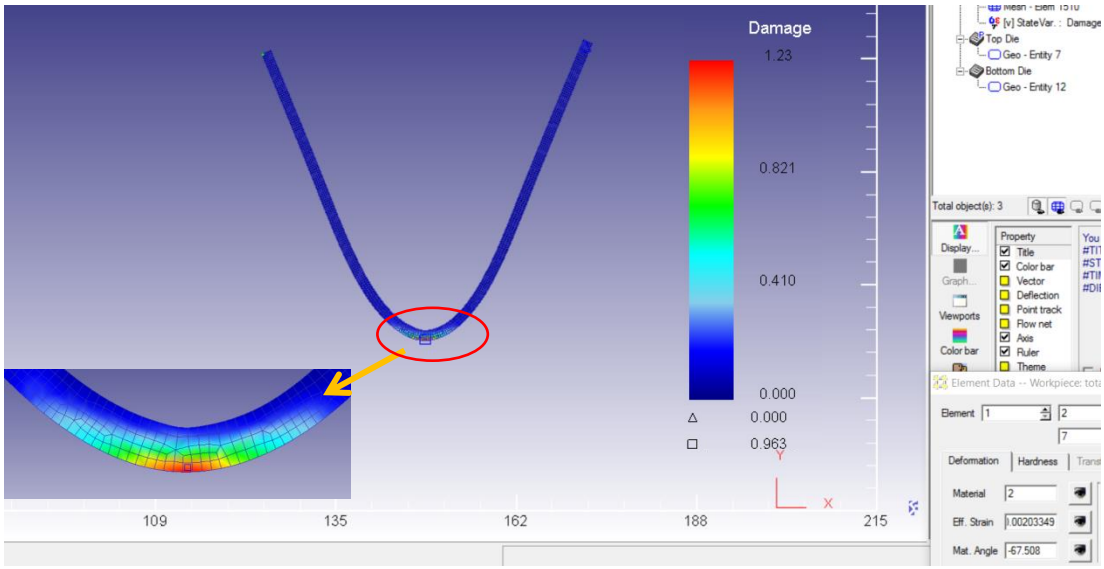

Figure 6.19 Locally Heated Bent Specimen with Angle of 45° in Deform™ 2D.

Load stroke diagram of locally heated AZ91B for V-bending process is shown in Figure 6.20. Bending load is low and almost same until the specimen reaches to 60^{o} bend angle. After that the contact areas between the specimen and the bottom die are increased, so that the friction force is increased. This can also be seen clearly in graph of thickness distribution on the bent area of the specimen (see Figure 6.22). More thinning is observed where the contact friction is higher. Additionally, heating the workpiece increases friction coefficient and therefore increases the friction load. Hence, punch load for bending operation increases.

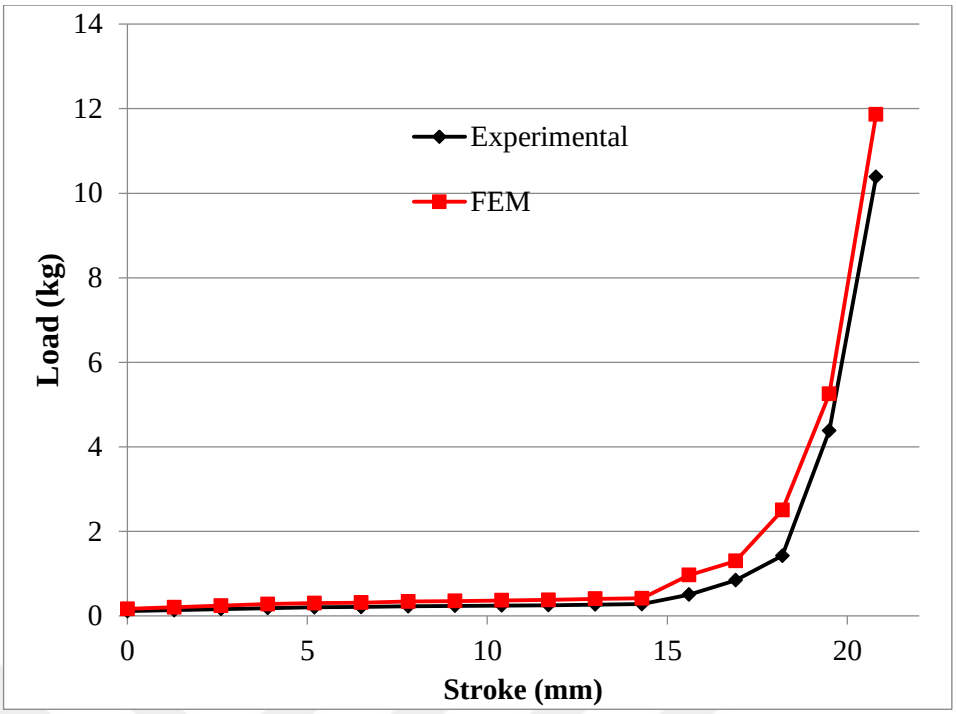

Figure 6.20 Load-Stroke Diagram of Locally Heated AZ91B

Load prediction has been created by Deform^{TM} 2D is always higher than experimental load which has been read from load cell. This differences may come from lubrication condition.

Springback is defined as recovery due to causes from elastic stresses remaining in the bend area during bending operation. Springback is related with punch angle, grain direction of sheet metal, die opening, sheet thickness, punch nose radius and punch height. Springback in experimental result are higher than FEM results. Difference in springback angles in experimental studies of AZ19B were sourced from original sheet thickness variation ($1{,}5^{+0{,}1}_{+0{,}05}$). The thickness of materials is exactly 1.5 mm in finite element analysis. It is known that the increasing in sheet thickness results in more springback after bending operation [39]. The amounts of springbacks are higher in locally heated specimens (due to increasing ductility) than cold ones. Therefore, the amount of over bending has to be taken bigger for warm bending during die design.

The experimental result obtained from cold and locally heated bending operations were compared in Table 6.2 and Table 6.3.

Table 6.2 Comparison of Locally Heated Bending and Cold Bending

EXPERIMENTAL RESULTS			
Angle of Bend	After Springback	Cold Bending (20°C)	Locally Heated Bending (150°C)
90	94/96		
75	77/78		
60	-/63		
45	-/47		

Table 6.3 Comparison of Locally Heated Bending and Cold Bending in Deform™ 2D

FINITE ELEMENT MODELLING RESULTS			
Angle of Bend	Final Angle For Cold Bending/Locally	Cold Bending(20°C)	Locally Heated Bending (150°C)
90	94/95	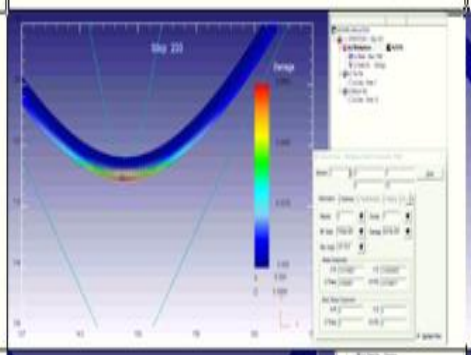	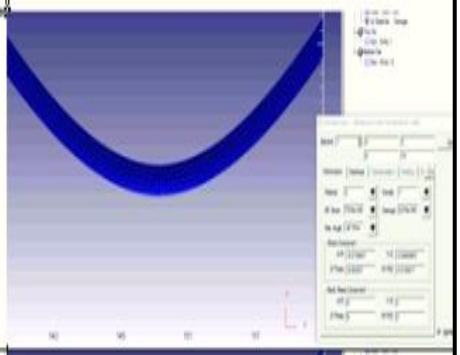
75	76/77	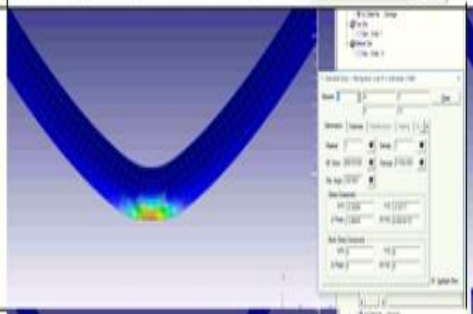	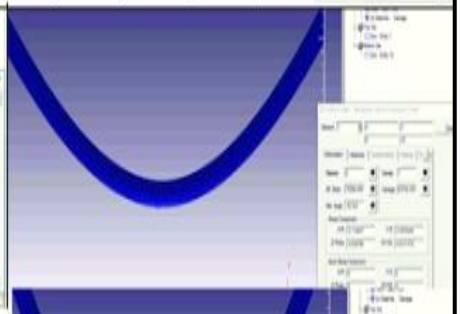
60	-/62	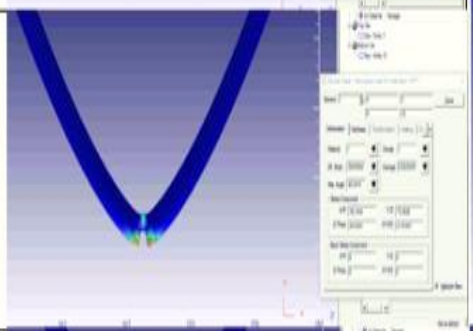	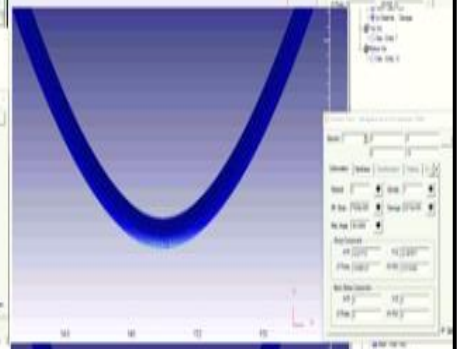
45	-/46	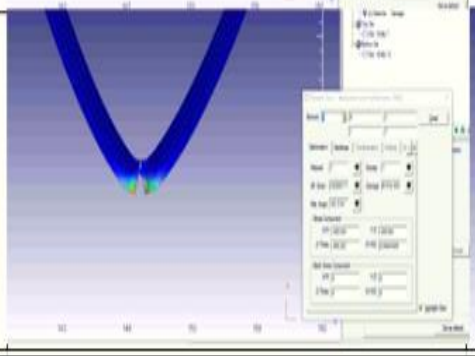	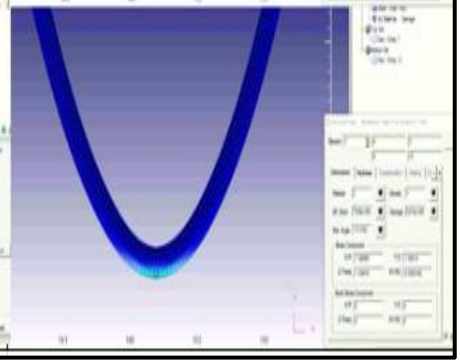

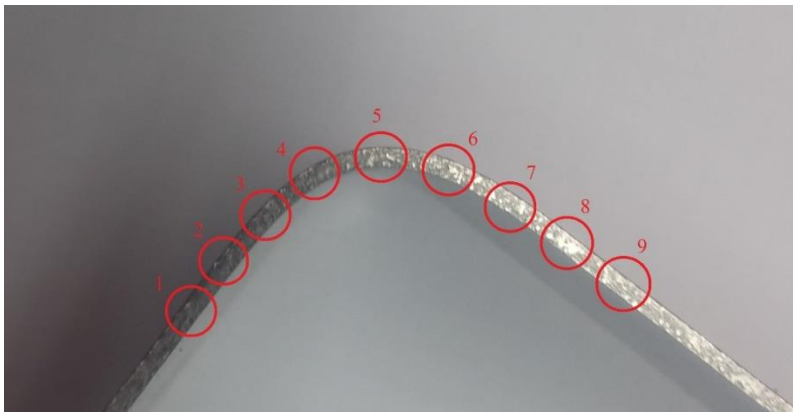

Figure 6.21 Certain Points on Specimen to Measure Thickness

The variations of the thickness of the specimens were measured on equally spaced points on the workpiece before and after bending operation (see Figure 6.21). Thickness is changing in the bend area depending on the amount of bend angle. Thinning is very effective in the nose of the bent specimen. The parameters influences thinning are die shoulder radius, punch nose radius, radial clearance, blank holder force and friction coefficient between workpiece and die. The difference in thickness distribution for cold bending and locally heated bending can be caused mainly from load distribution.

Figure 6.22 show the thickness reductions of AZ91B for cold and locally heated specimens. These measurements were achieved by using ultrasonic measuring devive.

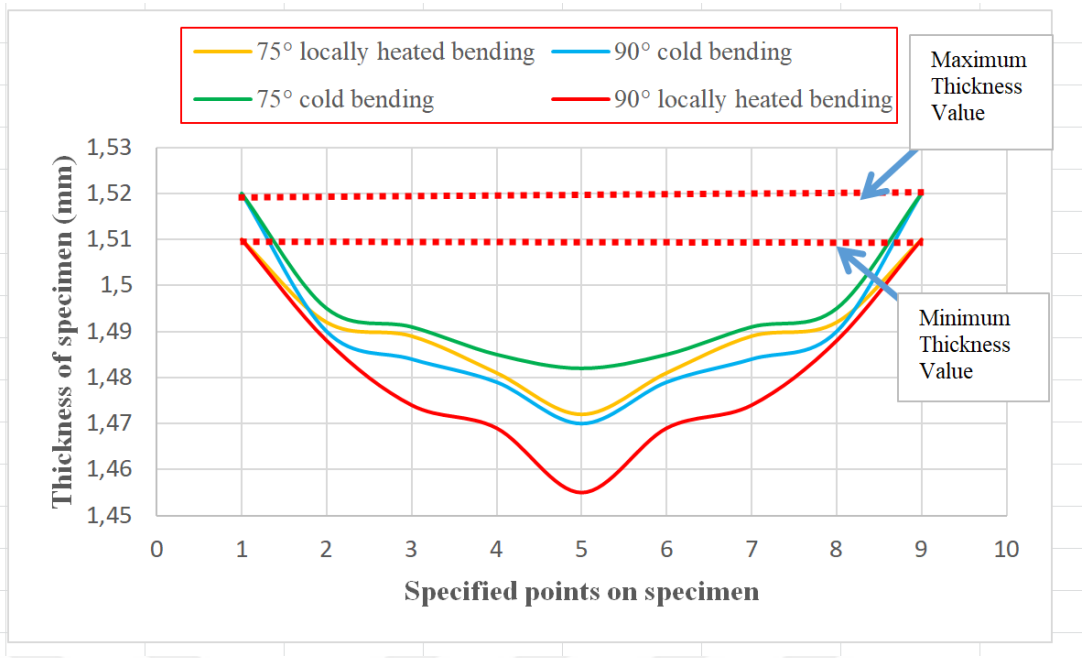

Figure 6.22 Graph of Thickness Distribution of AZ91B after Locally Heated and Cold Bending

6.2 Experimental and Finite Element Results for 1.4003 Bending

The cracks were formed on 90° cold bending of 1.4003 stainless steel specimens. It was expected because the corresponding bend radius is lower than the minimum radius value (R_{min}). It is recommended that minimum bend radius of 1.4003 stainless steel should not be smaller than the sheet thickness [36]. The bent angle measurement of FARO Prime FaroArm coordinate measuring machine (CMM) and the photograph of the specimen are shown in Figure 6.23. The bending cracks were observed at angle of $87°57'49.11''$ as shown in Figure 6.24.

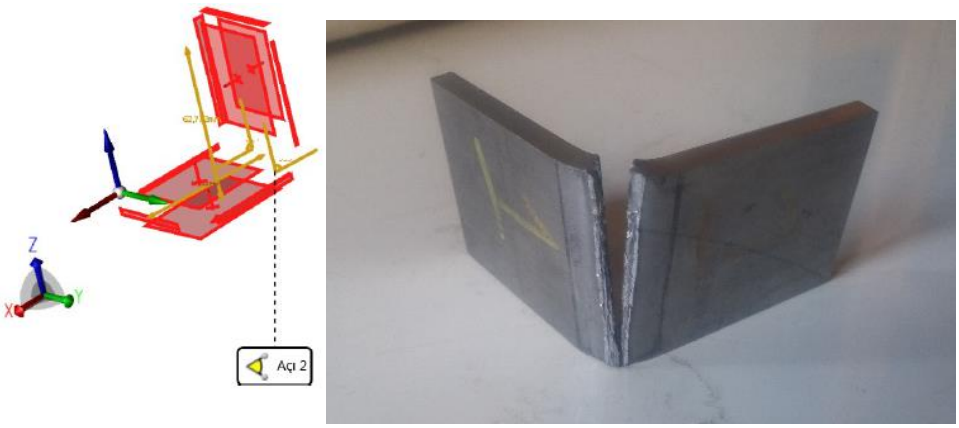

Figure 6.23 Illustrations of Formed Workpieces Measured by CMM and Cold Bent Workpiece.

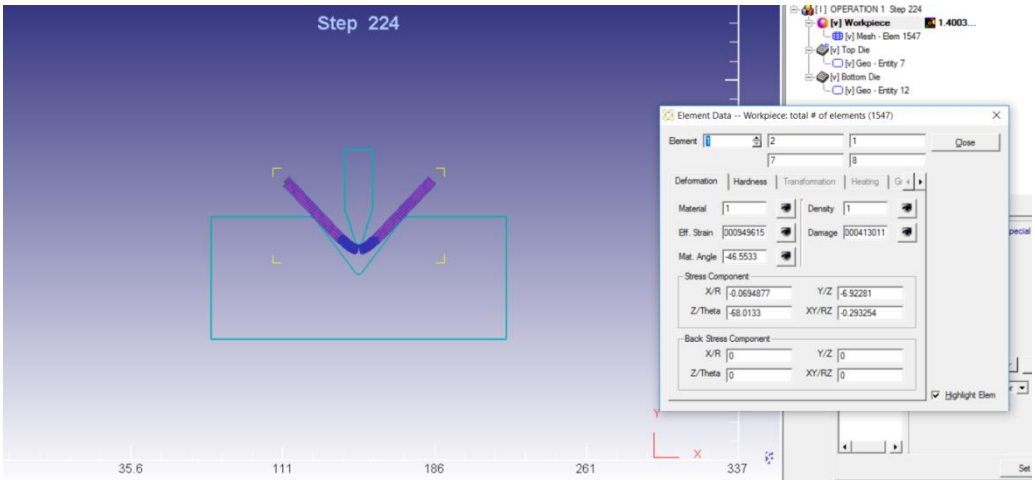

Figure 6.24 Illustration of Cold Bending of 1.4003 Final Angle in Deform™ 2D

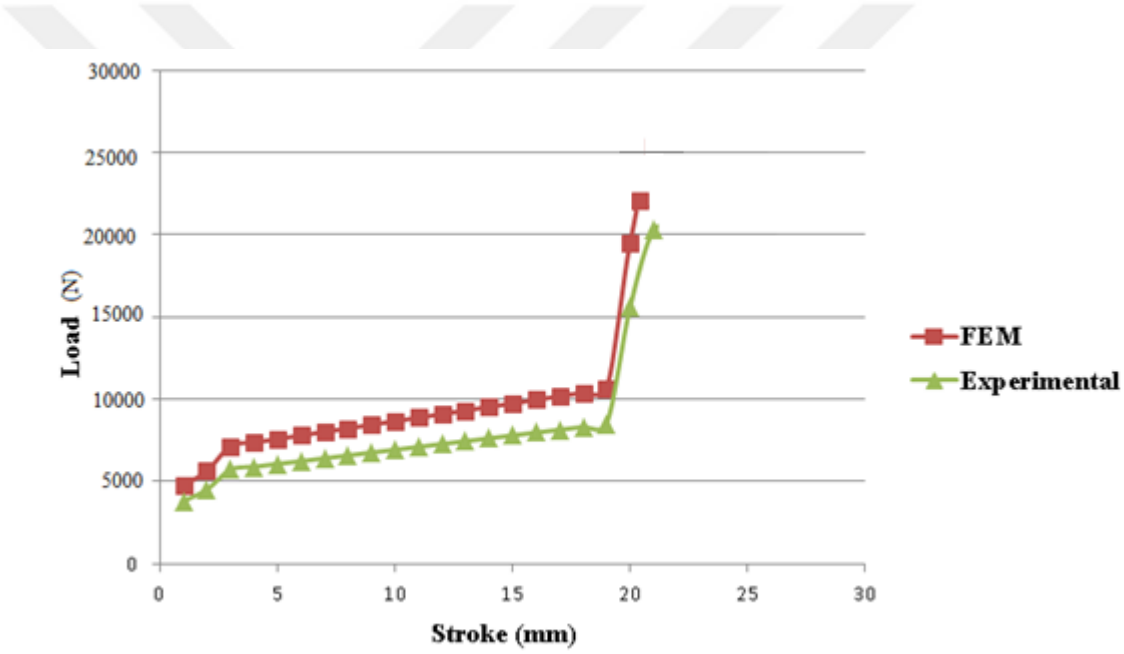

Figure 6.25 Load Stroke Diagram of Cold Bending of 1.4003

The load stroke curves obtained from experimental work and FEA for cold bending of 1.4003 specimens are given in Figure 6.25. As it was shown there are little differences in bending loads between experimental work and Deform™ 2D simulations. The difference in load is due lubrication (i.e. friction coefficient).

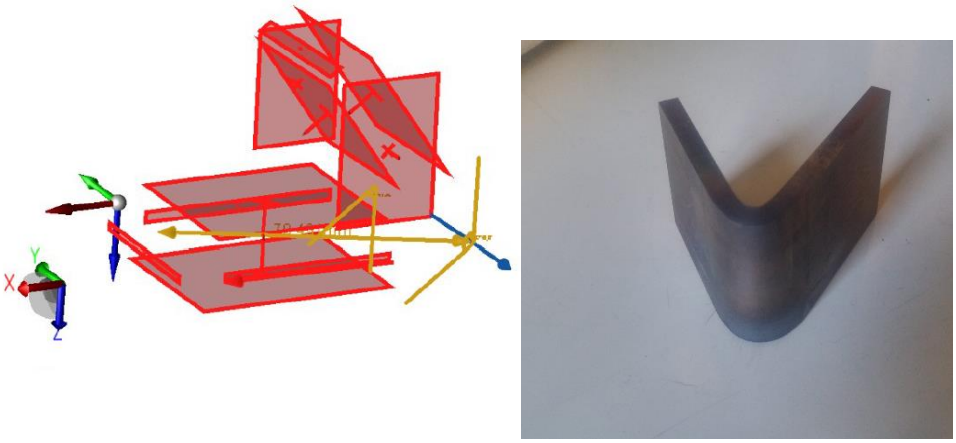

Figure 6.26 Illustration of Formed Workpieces Measured by CMM and Bent Workpieces After Locally Heating.

Cracks were not observed in locally heated specimens even 54 ° due to increasing ductility (temperature) on bending area.

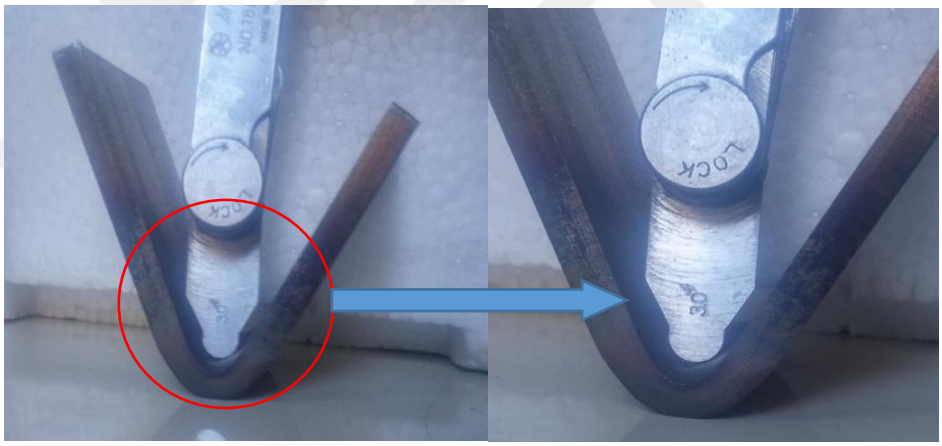

Figure 6.27 Radius measurement of 1.4003 After Bending Operation

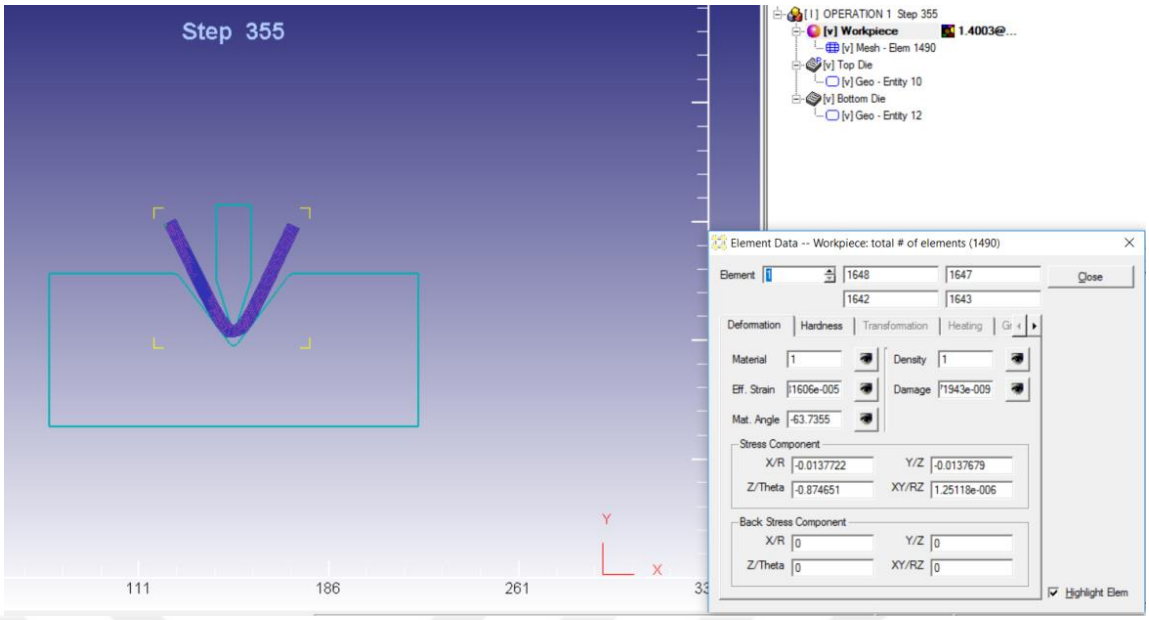

Figure 6.28 Illustration of Locally Heated 1.4003 Final Angle in Deform™ 2D

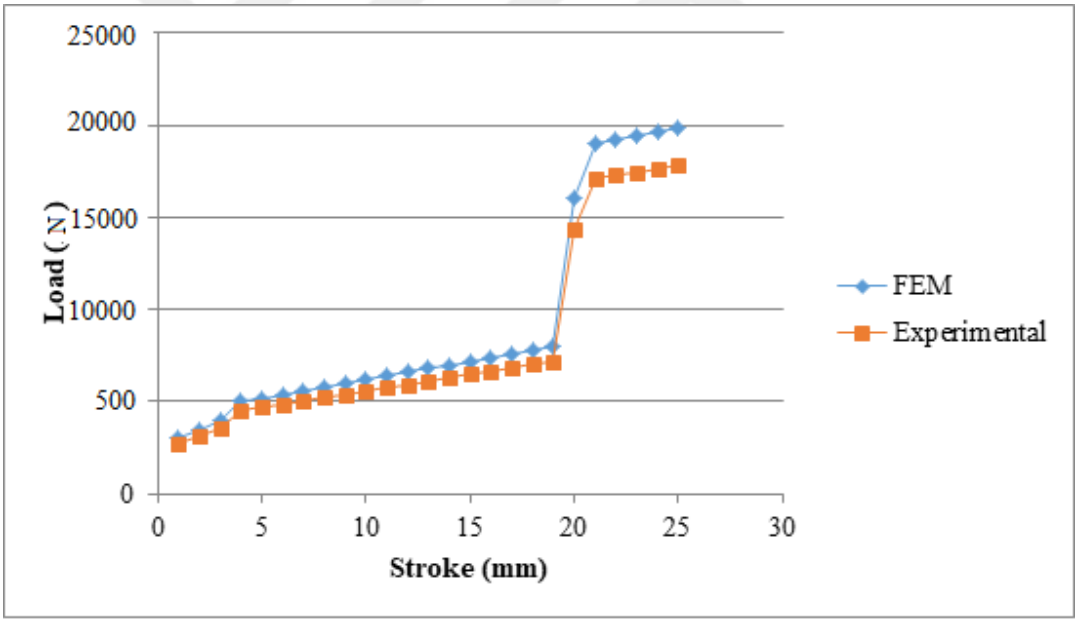

Figure 6.29 Load Stroke Diagram of Locally Heated 1.4003

The load stroke curves obtained from experimental work and FEA for locally heated 1.4003 specimens are given in Figure 6.29. The difference in bending loads between experimental work and Deform™ 2D simulations is because of lubrication (i.e. friction coefficient). The maximum load is lowered from 22500 N (cold bending) to 20000 N in locally heated specimens.

CHAPTER 7

CONCLUSIONS AND FUTURE WORKS

The finite element modelling and experimental investigations of sheet metal bending process have been presented in the previous chapters. After considering all the facts listed throughout the thesis, the following conclusions may be drawn:

- In this study, formability problem of the workpiece which is difficult to cold bend was overcome successfully by locally heating the bending area of workpiece.
- The FE model and experimental results are in well agreement.
- It was proven that warm forming is adequate for heat workpiece to give a shape for AZ91B (150^0C) and 1.4003 (600^0C).
- It was observed that thinning on workpiece is directly related with increasing temperature for AZ91B.
- The amount of springback is higher in locally heated specimens (due to increasing ductility) than cold ones. Therefore, the amount of over bending has to be taken bigger for warm bending during die design.

The following subject and parameters can be examined for further investigations about this study:

- The experimental study can be performed on AZ31B or AZ61B by locally heating only the outer bending side of workpiece.
- Forming operations can be carried out by using different forming rates and more complex shapes.
- Same study can be conducted with different friction coefficient conditions.
- The amount of overbending can be investigated for warm bending operation.
- Different heating procedure may be used for industrial practice.

REFERENCES

[1] Anttila S., Hannu-Pekka H. 2013. Structural Applications of Ferritic Stainless Steels. Luxembourg: RFCS Publications.

[2] Saha, P., Bhanja, A. (2013). Applications of Stainless Steel in Automobile Industry. *Advanced Materials Research.* **794**, 731–740.

[3] Mustafa Kemal, K. (2008). Magnesium and its alloys applications in automotive industry. *The International Journal of Advanced Manufacturing Technology*. **39**, 851–865.

[4] Yoshihara, S., MacDonald, B., Nishimura, H., Yamamoto, H., Manabe, K. (2004). Optimisation of magnesium alloy stamping with local heating and cooling using the finite element method. *Journal of Materials Processing Technology*. **1**, 319–322.

[5] Lee, E., Hwang, J., Lee, W., Yang, Y., Yang, W. (2014) A local heating method by near-infrared rays for forming of non-quenchable advanced high-strength steels. *Journal of Materials Processing Technology*. **214**, 784–793.

[6] Hino, R., Yoshida, F., Nagaishi, N., Naka, T. (2008).Incremental Sheet Forming With Local Heating for Lightweight Hard-To-Form Material. *International Journal of Modern Physics B.* **22**, 6082–6087.

[7] Kim, S., Lee, Y., (2014). Comparative study on failure prediction in warm forming processes of Mg alloy sheet by the FEM and ductile fracture criteria *Metallurgical and Materials Transactions B*. **45**, 445–453.

[8] Tokita, Y., Nakagaito, T., Tamai, Y., T, Urabe. (2017). Stretch Formability of High Strength Steel Sheets in Warm Forming. *Journal of Materials Processing Technology*. **246**, 77–84.

[9] Ebrahimi, G., Maldar, A., Monajati, H., Haghshenas, M. (2012). Hot deformation behavior of AZ91 magnesium alloy in temperature ranging from 63

350°C to 425°C. *Transactions of Nonferrous Metals Society of China.* **22**, 2066–2071.

[10] Bong, H., Ahn, D., Kim, Y., Lee M. (2013). Formability of austenitic and ferritic stainless steels at warm forming temperature. *International Journal of Mechanical Sciences*. **75**, 94–109.

[11] Mabuchi, M., Iwasaki, H., Yanase, K. Higashi, K. (1997). Low temperature superplasticity in an AZ91 magnesium alloy processed by ECAE. *Scripta Materialia*. **36**, 681–686.

[12] Zhang, K., Yin, D., Wu, D. (2006). Formability of AZ31 magnesium alloy sheets at warm working conditions. *International Journal of Machine Tools and Manufacture.* **46**,1276–1280.

[13] Ji, Y., J, Park., (2008). Formability of magnesium AZ31 sheet in the incremental forming at warm temperature. *Journal of Materials Processing Technology.* **201**, 354–358.

[14] Al-Zubaydi, A., Zhilyaev, A., Wang, S., Reed, P. (2015). Superplastic behaviour of AZ91 magnesium alloy processed by high-pressure torsion. *Materials Science and Engineering*. **637**, 1–11.

[15] Kim, H., Kim, W. (2010). Failure prediction of magnesium alloy sheets deforming at warm temperatures using the Zener-Holloman parameter. *Mechanics of Materials*. **42**, 293–303.

[16] Quan, G., Liang, J., Lv, W., Wu, D., Liu, Y. (2014). A Characterization for the Constitutive Relationships of 42CrMo High Strength Steel by Artificial Neural Network and its Application In Isothermal Deformation. *Journal of Materials Research.* **17**, 1102–1114.

[17] Viatkina EM, Brekelmans WAM, Geers MGD. Forming limit diagrams for sheet deformation processes. 2001. http://repository.tue.nl/df9c4dcc-b2c2-43ef-8f6f-608b4f29533d. Accessed May 13, 2017.

[18] Sheet Metal Forming. 2017. http://www.custompartnet.com/wu/sheet-metal-forming#bending. Accessed 17.06.2017.

[19] Sheet Metal Forming. 2017. http://www.custompartnet.com/wu/sheet-metal-forming. Accessed 15.06.2017.

[20] Serope, K., Schmid, R., Musa, H. 2009. Manufacturing Engineering and Technology. 7th edition. The University of Notre Dame: Pearson.

[21] Spring Back. 2017. http://sheetmetal.me/tooling-terminology/spring-back. Accessed 15.06.2017.

[22] Shi, C. (2013). Preface from Honorary Editor in Chief. *J. Magnes. Alloy.*,**1**, 1.

[23] Paristech, M. (2012). École nationale supérieure des mines de Paris Numerical and experimental study of AZ31-O magnesium alloy warm sheet forming. *Sciences de l'ingénieur*.1.1.

[24] Ostrovsky, L., Henn, Y. (2007). Present state and future of magnesium application in aerospace industry. *Int. Conf. "New Challenges Aeronaut. ASTEC 07.***1**,5.

[25] ASTM. American Society for Testing and Materials. 1997. Standard Specification for Zinc and Zinc-Aluminum (ZA) Alloys in Ingot Form. 41. p. West Conshohocken. 10.1520/B0240-13.

[26] Berat, B., Aydın, S., İskender, Ozkul. Investigation of Magnesium Alloys Machinability. *International Journal Of Electronics; Mechanical And Mechatronics Engineering.***2**, 261–268.

[27] AZOM. The A to Z of Materials. 2017. Magnesium AZ91B-F (UNS M11912) Die Cast Alloy. 2017. http://www.azom.com/article.aspx?. 20.05.2017.

[28] Iwanaga, K., Tashiro, H., Okamoto, H., Shimizu, K. (2004). Improvement of formability from room temperature to warm temperature in AZ-31 magnesium alloy. *Journal of Materials Processing Technology*. **155**, 1313–1316.

[29] Peng, Q., Ji, W., Huang, H., De, S. (2013). Axial ratio dependence of the stability of self-interstitials in HCP structures. *Journal of Nuclear Materials.* **437**, 293–296.

[30] Britton, T., Dunne, F., Wilkinson, J. (2015). On the mechanistic basis of deformation at the microscale in hexagonal close-packed metals. *Proceedings of the Royal Society.* **471**,20140881.

[31] Lou, X., Li, M., Boger, K., Agnew, S. Wagoner, R. (2007). Hardening evolution of AZ31B Mg sheet. *International Journal of Plasticity.* **23**, 44–86.

[32] DoITPoMS - TLP Library Slip in Single Crystals - Slip geometry. 2017.

https://www.doitpoms.ac.uk/tlplib/slip/slip_geometry.php. Accessed 13.05.2017 .

[33] Marco Boniardi, Andrea Casaroli. 2014. 1st edition. Stainless steels. Brescia: Lucefin.

[34] Cunat, P. (2004). Alloying elements in stainless steel and other chromium-containing alloys. *International Chromium Development Association.***1**, 1–24.

[35] Outokumpu, "Handbook of Stainless Steel," *Sandvikens Tryckeri*, pp. 1–89, 2013.

[36] Paper, C., Kong, H. (2016). Material Properties Of Cold-Formed Ferritic Stainless Steel At Elevated. *Eighth International Conference on Advances in Steel Structures.* **1**, 0–12.

[37] Kvačkaj T, Tiža J, Bacsó J, (2014). Cockcroft-Latham Ductile Fracture Criteria for Non Ferrous Materials. *Mater Sci Forum*.; doi:10.4028/www.scientific.net/MSF, **782**, 373.

[38] Mihriban, P., Karl, K., Arslan, K. 2013. Fundamentals of Magnesium Alloy Metallurgy. First Edition, Sawston: Cambridge. 2013.

[39] Gite,R., Bajaj, D. (2016). Spring Back Effect Analysis of Bracket Using Finite Element Analysis. *International Engineering Research Journal*. **3**, 246–255.